



www.viserdata.com

RESEARCH AND APPLICATION OF **MATERIALS SCIENCE**

ISSN 2661-4464(online) 2661-4456(print)

Volume 6 No. 1 2024



Research and Application of Materials Science

Editor-in-Chief: Zidong Wang

Associate Editors: Yong Zhang Ting Zhu Junfei Ou Jing Wang

Editorial Board Members:

| | | | | |
|--------------|----------------|---------------|----------------|----------------|
| Wencai Zhang | Zhenguo Nie | Chunjuan Cui | Xu Hou | Zesong Wang |
| Liangyu Chen | Shuoping Chen | Zunli Mo | Chaogui Tan | You Wang |
| Di Yun | Lizhao Qin | Wenlong Zhou | Shuquan Liang | Jinping Xiong |
| Jun Wang | Donghong Wang | Lei Fan | Sheng Han | Xiehong Cao |
| Dongbin Fan | Zhimin Wu | Mingchun Zhao | Chunchang Wang | Zhongliang Shi |
| Yude Liu | Jiangyong Wang | Haiyan He | Yanxin Qiao | Chichong Lu |
| Kaihui Nan | Zongrui Liu | Zegao Wang | Lihua Zhu | Linbo Li |
| Shidong Zhu | Huanggen Yang | Jizhong Song | Xifeng Ding | Yongfeng Shen |
| Liyang Wang | Zexing Wu | Wenli Gao | Xianyou Wang | Hongji Liu |
| Xiuli Zhang | Yandong Wang | Quanbing Liu | Qing Wang | Shuo Zhao |
| Jiming Zhang | Zhiguo Wang | Huaqing Li | Chaofeng Zhang | Chenguang Hu |
| Wei Liu | Jiankang Huang | Shaohua Luo | Suyun Tian | Yumin Huang |
| Hui Li | Xinli Guo | Jiangmiao Yu | Xiaowei Zhang | Yuanfu Deng |
| Dengfeng Yin | Zhigang Yang | | | |



Publisher: Viser Technology Pte. Ltd.

ISSN: 2661-4464(online)

2661-4456(print)

Frequency: Semi-annual

Add.: 21 Woodlands Close, #08-18

Primz Bizhub SINGAPORE (737854)

https://www.viserdata.com/

Editors:

Yajun Lian Yanli Liu

John Wilson Nike Yough

Mart Chen Qiuyue Su

Debra Hamilton Xin Di

Jennifer M Dohy Xiuli Li

Edward Adam DavisLiangjun Qiu

Designer: Anson Chee

Research and Application of Materials Science

Volume 6 No.1 (2024)

CONTENTS

| | |
|---|-----------|
| The Effect of Graphene Oxide on Mechanical Properties of Cement Mortar | 1 |
| Lei FAN, Jinhao ZHENG | |
| Research on Heredity of Coarse Ferrite Grains..... | 5 |
| Wangzhan FAN, Weimin GUI, Youfeng CHEN | |
| High Temperature Rheological Performance of Graphene Modified Rubber Asphalt | 9 |
| Heyuan GUO, Chunhua LI, Xin ZHAO, Yinghua YUAN, Shaoqi TANG, Yongjun MENG | |
| Research Progress of High Entropy Ceramic Materials | 16 |
| Song WU, Shikai LIU, Jialin WANG, Bibo HAN, Shaoyi SHEN, Zhigang YU, Zhaobo ZHANG, Xinhua ZHENG | |
| Research Progress of Non-oxide and High Entropy Ceramic Coatings..... | 23 |
| Junshuai CHEN, Yulong WANG, Zeyu WANG, Xue SHEN, Tengyu DU, Yubo GONG, Zhigang YANG, Gang YU | |
| Research and Application of Recycled Concrete Technology in Prefabricated Buildings..... | 33 |
| Shanshan DENG, Gang SHI, Chao SHANG, Fuchuan ZHOU, Masabo Gasper, Masiko M. Kaziana | |

The Effect of Graphene Oxide on Mechanical Properties of Cement Mortar

Lei FAN^{1,2}, Jinhao ZHENG^{1,2}

1. School of Civil Engineering and Architecture, Zhejiang University of Science & Technology, Hangzhou, Zhejiang, 310023, China
2. Zhejiang- Singapore Joint Laboratory for Urban Renewal and Future City, Hangzhou, Zhejiang, 310023, China

*Corresponding Author: Lei FAN, E-mail: fanleigl@foxmail.com

Abstract

Cement is widely used in engineering applications, but it has both the characteristics of high brittleness and poor bending resistance. In this paper, the effects of different amounts of graphene oxide on the flexural strength and compressive strength of cement mortar were studied by doping a certain amount of graphene oxide with cement mortar, and the strengthening mechanism of graphene oxide on cement mortar was obtained through microstructure detection. It is found that graphene oxide has a significant enhancement effect on the macroscopic mechanical properties of cement mortar, and graphene oxide provides nano-nucleation sites and growth templates for cement mortar, accelerates the hydration process, reduces the voids between hydration products, greatly increases the compactness, and improves the macroscopic properties of cement-based materials.

Keywords: Graphene oxide; Cement mortar; Mechanical properties; Microscopic analysis

1 Introduction

Cement is an essential material component in the construction of engineering buildings^[1]. When cement is mixed with other building materials, it forms a high-strength cement mortar^[2]. However, its own characteristics such as high brittleness and poor bending resistance restrict the performance of construction projects^[3]. Therefore, improving the performance of cement-based materials has become a research hotspot for scholars at home and abroad. The mechanical properties of cement-based materials mainly depend on the ratio of aggregate, water, cement and the amount and shape of hydration products formed^[4]. Many scholars use reinforcing materials such as steel bars, glass fibers, and polypropylene fibers to achieve the purpose of improving cement-based materials, but these materials can only inhibit the generation of cracks at the macro and micro scales, and cannot affect the shape and quantity of hydration products, and cannot do anything about nanoscale cracks^[6].

Graphene oxide, known as an oxide of graphene, has entered the field of vision of scholars with more activity and can improve the material properties through oxygen-containing functional groups. Lu Shenghua et al^[6-7] Graphene oxide was prepared by improved Hummers method and ultrasonic dispersion method, and mixed into cement slurry, and its

microscopic morphology was observed by scanning electron microscopy (SEM), and it was found that graphene oxide had a promoting effect and template effect on the formation of cement hydration crystal products, and could promote the formation of neat and regular flower-like nanocrystals in cement hydration products, so as to achieve the effect of enhancing toughening. Zhu Pan et al^[8]. The mechanical properties of ordinary Portland cement with graphene oxide were studied, and combined with the images under the scanning electron microscope, it was found that the addition of graphene oxide improved the pore structure of the cement-based materials, and made the cement hydration process form a strong interfacial force, thereby greatly improving the mechanical properties of the cement-based composites.

In 2023, Team Lei Fan^[9] used the large-scale Atoms/Molecular Parallel Simulator (LAMMPS) to confirm that carbon nanotubes (CNTs) enhance the interfacial interaction and overall coherence of double graphene oxide (GO) layers and calcium silicate hydrate (CSH) matrix, despite a slight marginal deterioration in tensile strain. Adding one CNT increases the normalized pull-out energy ($E_{pull-out}^{nor}$) and normalized shear stress (τ_{shear}^{nor}) values of the D-GO/CSH model by 24.56% and 25.93%, respectively. Furthermore^[10], incorporating hexagonal boron nitride (hBN) nanosheets with defect sizes enhances the interfacial interaction between hBN and the CSH matrix compared to pure hBN-reinforced

CSH nanostructures. Specifically, introducing defective hBN with an R3 defect size of 17.275 Å boosts failure strain and stress by 35.53% and 31.58%, respectively. In 2024^[11], demonstrated that employing sp³ bonds, different functional group types, and chirality can augment the interfacial interaction between CSH and GO. The $E_{pull-out}^{nor}$ and τ_{shear}^{nor} of the OH-sp³ model increase by 44.93% and 49.25%, respectively, compared to the control group, while those of the zigzag-cen model increase by 12.36% and 9.89%, respectively. Wang. Z M, et al.^[12] conducted mechanical property tests on GO-modified cement mortar. The results showed that the highest compressive and indirect tensile strength of cement mortar at 28d were enhanced by 13.1% and 41.3%, respectively, after the incorporation of GO. Lv. S H, et al.^[13] Investigated the effect of graphene oxide of different sizes and contents on the shape of cement hydration crystals and the strength of cement paste, and found that the graphene oxide could promote the formation of rod-like crystals and polyhedral structures, which made the cement paste denser. Long. W J, et al.^[14] showed that after doping 0.05% and 0.2% of GO, the compressive and flexural strengths of cementitious composites were increased by 12-26% and 2-20%, respectively, at the age of 28d. For this reason, we investigated the effect of graphene oxide on cement mortar, and explored the strengthening mechanism of graphene oxide on cement mortar based on two different scales: macro and micro.

2 Experimental Studies

2.1 Raw materials

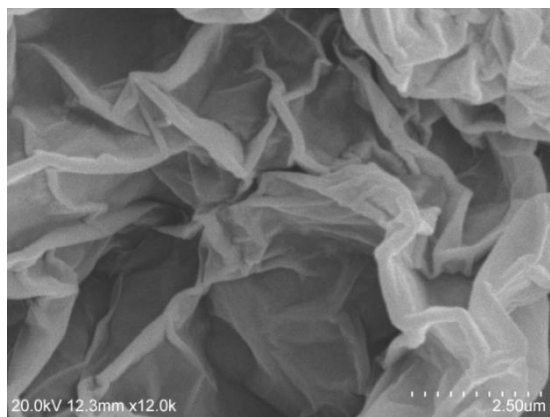


Figure 1 Graphene oxide microstructure diagram

In this experiment, Conch brand P O42.5 grade ordinary Portland cement was used, the main physical indexes are shown in Table 1, the sand used is river sand, the particle size is 0.01-4mm, the fineness modulus is 2.7, the water reducer is FK-A polycarboxylic acid high-performance superplasticizer powder, the water reduction rate is 26%, the graphene oxide is SH-GO-1280 type graphene oxide, which is prepared by

the improved Hummers method, the thickness is $\sim 1\text{nm}$, the oxygen content is $>54\%$, and the purity is 99.9%, the peelability rate is 99%, and the graphene oxide microstructure is shown in Figure 1.

2.2 Preparation process

2.2.1 Dispersion preparation

Preparation of graphene oxide standard dispersion: first take the whole mass of polycarboxylate superplasticizer (cement mass fraction is 0.6%) and put it in a 500ml beaker, add deionized water (0.35 times the mass of cement), and stir thoroughly until no agglomeration appears. Graphene oxide with cement mass fractions of 0.02%, 0.05% and 0.08% was weighed and added to the evenly mixed superplasticizer solution, and the magnetic heating mixer was used to stir evenly for 10 min. Then, it was dispersed in an ultrasonic cleaner (JP-040S) for 20 min to obtain a graphene oxide standard dispersion.

2.2.2 Specimen preparation

The standard dispersions of graphene oxide with different dosages were controlled separately, and the fixed water-cement ratio was 0.35, and the cement mortar specimens without graphene oxide were used as the control group, and a total of 4 groups were set up.

Accurately weigh the corresponding quality of cement and river sand, now mix the cement with graphene oxide standard dispersion and stir slowly with a cement mortar mixer for 30 s, then pour river sand, slow stirring for 1 min, high-speed stirring for 2 min, in accordance with GB/T17671-1999 "Cement Mortar Strength Test Method (ISO Method)" on the cement mortar vibrating table, the frequency is 60 times/min, the vibrating is 2 min, and the compaction is formed. Demold within 20~24 h and put it into a standard curing box for curing.

2.2.3 Test methods

According to GB/T17671-1999 "Cement Mortar Strength Test Method (ISO Method)", the compressive strength and flexural strength of each group of specimens are tested in 3D. The cross-section of the specimen that has undergone 3D flexural strength and compressive strength tests was observed and tested with SU1510 scanning electron microscope.

3 Test Results and Analysis

3.1 Experimental macroscopic observation

In the process of preparing cement mortar, under the premise of a certain ratio, with the continuous increase of graphene oxide content, the experimental group showed poor fluidity, increased viscosity, and darkened color of cement mixture. Mainly because the specific surface area of graphene oxide is much larger than that of cement, the water consumption of cement mortar increases significantly with the increase of graphene oxide content

in the case of consistent water-cement ratio.

3.2 Macroscopic mechanical properties

The compressive strength and flexural strength of graphene oxide in 3D were recorded in different amounts. After the addition of graphene oxide, the 3D compressive strength and flexural strength of cement mortar were increased by 8.87% and 8.11%, respectively, and the compressive strength and flexural strength increased by 16.8% and 12.36%, respectively. It can be found that when the content of graphene oxide in cement mortar is within a certain range, increasing the content of graphene oxide can significantly improve the macroscopic mechanical properties of cement mortar. This is because graphene oxide can promote the formation of more hydration products of different shapes in cement, fill the cracks at the nanoscale, inhibit development, and act as a link in the cement hydration products.

3.3 Microscopic analysis

In this experiment, SEM microscopy was carried out on the cross-sections of cement mortar with different graphene oxide dosage in the control group with an age of 3 days, and the results are shown in Figure 2.

Figure 2a and 2b are the microstructure scans of the cement mortar control group, and it can be observed that the connections between the hydration products of the cement mortar control group are relatively scattered, and the hydration products are mostly flower cluster crystals and the distribution and stacking are relatively random, resulting in a large number of voids between the crystals inside the cement matrix. Figure 2c and 2d are microscopic scans of cement mortar doped with a small amount of graphene oxide, and it can be observed that the volume of the granular crystal hydration products of cement increases significantly after a small amount of graphene oxide is added, and these crystals are stacked on top of each other and distributed more evenly. This is because graphene oxide acts as a nano-nucleation site, which accelerates the hydration process. Figure 2e and 2f are microscopic scans of cement mortar with increased graphene oxide dosage, and the directional rod-like structure of C-S-H and C-H phases is formed in the cement. These rod-like structures act as a link and act as a bridge in the hydration products, with significantly reduced voids compared to the control group. Figure 2g and 2h are the microscopic scans of cement mortar after the further increase of graphene oxide incorporation, and it can be found that the hydration products appear in the regular C-H phase block and polyhedral state, and the needle rod crystals are significantly reduced. This is due to the fact that graphene oxide provides a growth template for cement mortar and makes the hydration products intertwine and penetrate into a dense and uniform microstructure during the aggregation process, which significantly improves the strength of cement mortar.

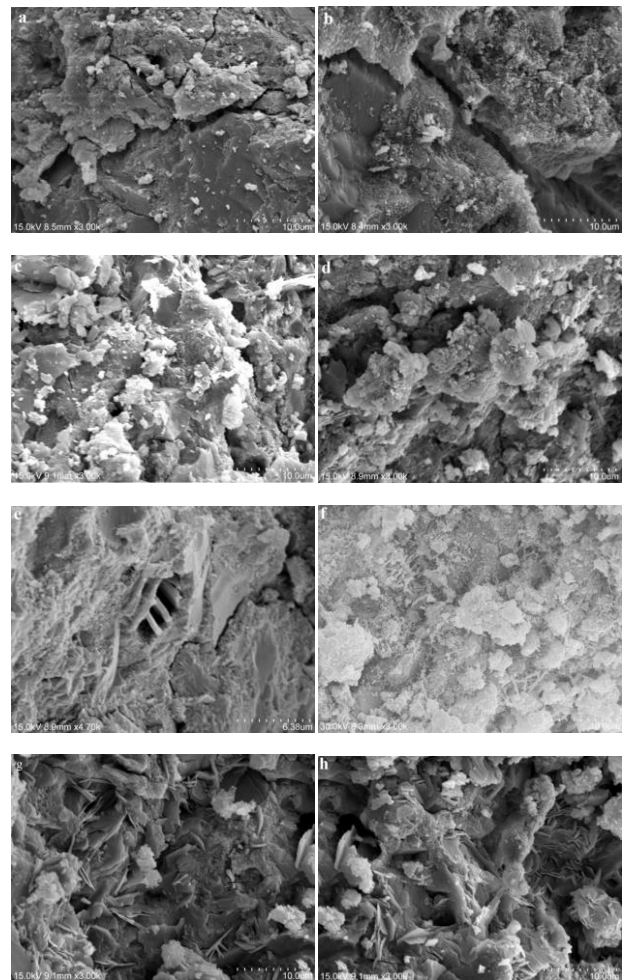


Figure 2 (a) (b) cement mortar control group, (c) (d) cement mortar test group mixed with some GO, (e) (f) cement mortar test group with increased GO content, (g) (h) cement mortar test group with further GO content

4 Conclusion

The incorporation of graphene oxide leads to an increase in water consumption per unit of cement. If the water consumption is not increased or the use of superplasticizer is increased, the fluidity of the cement mortar will become poor, the viscosity will become larger, and the strength will be reduced.

In a certain dosage range, the macroscopic properties of cement mortar can be significantly improved by increasing the amount of graphene oxide, and the compressive strength and flexural strength can be increased by up to 16.8% and 12.36%.

The mechanism of action of graphene oxide reinforced cement mortar is to produce different shapes and more quantities of hydration products to increase the compactness of cement mortar and reduce porosity.

The microstructure and crystalline composition of hydration products greatly influence the macroscopic mechanical properties of cement-based materials.

Graphene oxide can promote the hydration process of cement mortar, and has a promoting effect on the properties and quantity of hydration products.

Acknowledgments: This work were supported by Natural Science Foundation of Zhejiang Province (LQ23E080003), a Doctoral program of Zhejiang University of science and technology (F701104L08) and The Special Fund Project of Zhejiang University of Science and Technology's Basic Scientific Research Business Expenses in 2023 (2023QN016).

Conflict of interest: No potential conflict of interest was reported by the authors.

5 References

- [1] He. X H and Han. J Y. Preparation and properties of graphene oxide modified concrete[J]. *Functional materials*, 2022,53(7):7169-7174.
- [2] Sun. J L, Zhou. X D and Niu. Z Q. Graphene oxide and functionalized carbon nanotubes enhance the mechanical properties of cement-based materials[J]. *highway*, 2022,67(9):365-373.
- [3] Xiang. X P, Liu. S Y , Zhang Y, et al. Study on the self-shrinkage mechanism of graphene-doped cement mortar[J]. *New building materials*, 2022,49(5):62-69.
- [4] Zeng. J J, Gao. Z Y, Ruan D. Performance and research progress of graphene oxide cement-based composites[J]. *Material Reports*, 2021,35(1):198-205.
- [5] Xu. Y H and Fang. Y F. Mechanical properties and fractal characteristics of microstructure of graphene oxide cement slurry[J]. *concrete*, 2020(8):130-134.
- [6] Lv. S H, Sun T and Liu. J J, et al. Toughening effect and mechanism of graphene oxide nanoflakes on cementitious composites[J]. *Journal of Composite Materials*, 2014,31(3):644-652.
- [7] Lv. S H, Ma. Y J, Qiu. C C and Ju. H B. Study of graphene oxide reinforced toughened cementitious composites[J]. *functional material*, 2013,44(15):2227-2231.
- [8] Zhu Pan, Li He, Ling Qiu, et al. Mechanical Properties and Microstructure of a Graphene Oxide-cement Composite[J]. *Cement & Concrete Composites*, 2015(58):140-147.
- [9] Fan L. Interlayer stress transfer improvement in bi-layer graphene oxide/calcium silicate hydrate via CNTs[J]. *Colloids and Surfaces A: Physicochemical and Engineering Aspects*, 2024,692:133904.
- [10] Fan L. A high improvement of tensile properties and interfacial interaction of calcium silicate hydrate/hexagonal boron nitride layered nanostructures via defect field[J]. *Computational Materials Science*, 2024,233:112675.
- [11] Fan L, Song F, Xu J, et al. Interlayer sp³ Bonds and Chirality at Bilayer Graphene Oxide/Calcium Silicate Hydrate Abnormally Enhance Its Interlayer Stress Transfer[J]. *ACS Omega*, 2024,9(9):10343-10352.
- [12] Wang. Z M and Zhang. H L. Study on the mechanical properties of graphene oxide nanosheet reinforced cement-based composites[J]. *Industrial buildings*, 2021,51(2):153-157.
- [13] Lv S H, Liu J J, Sun T, et al. Effect of GO nanosheets on shapes of cement hydration crystals and their formation process[J]. *Construction and Building Materials*, 2014,64:231-239.
- [14] Long W J, Wei J J, Xing F, et al. Enhanced dynamic mechanical properties of cement paste modified with graphene oxide nanosheets and its reinforcing mechanism[J]. *Cement and Concrete Composites*, 2018,93:127-139.

Research on Heredity of Coarse Ferrite Grains

Wangzhan FAN*, Weimin GUI, Youfeng CHEN

Shanxi Fast Gear Co. Ltd., Xi'an, shaanxi, 710119, China

*Corresponding Author: Wangzhan FAN, E-mail: 252985662@qq.com

Abstract

The changes in austenite grain size of the specimens with coarse ferrite grains under different heat treatment process were investigated. The focus was on studying the effect of annealing on refining coarse ferrite grains, as well as the influence of the ferrite grain size on the main technical indicators of gas carburizing. The results show that coarse ferrite grains may not necessarily cause the coarse austenite grains, but may result in mixed austenite grains. After annealing treatment, the coarse ferrite grains can be significantly refined and homogenized. Moreover, the coarse ferrite grains have no significant effects on hardness and intergranular oxidation of gas carburizing.

Keywords: grain size; coarse ferrite grains; austenite; gas carburizing

1 Introduction

The grain size has significant effects on the properties of metals and is determined by grain growth and grain refinement^[1]. Case hardening steels for automobile gears are generally inherent fine grain size. But during the forging process of the automobile gears, the phenomenon that the ferrite grains become coarser and resulting in the mixed grains still occasionally occurs. However, the gear blanks need to be heat treated such as normalizing, quenching and gas carburizing. During these subsequent heat treatment, whether the grain size of the gears will change and how the coarse ferrite grain size affects the austenite grain size, it is not clear. In this work, the changes of coarse ferrite grains after quenching or gas carburizing and the effects on the main technical indicators of gas carburizing are studied, as well as the changes of coarse grain size after annealing.

2 Experimental

2.1 Test materials

The specimens were taken from 20CrMnTiH3 hot rolled bars with a diameter of 80 mm. The chemical composition was listed in Table 1.

Table 1 Chemical composition of the specimens (wt. %)

| Grades | C | Si | Mn | P | S | Cr | Ti |
|------------|------|------|------|------|------|------|-------|
| 20CrMnTiH3 | 0.19 | 0.23 | 0.89 | 0.03 | 0.22 | 1.16 | 0.058 |

2.2 Test methods

(1) The bars with a diameter of 80 mm were heated to 1300 °C for 30 min, then forged into gear blanks, slowly cooled to room temperature. The specimen was taken from the outer circle of the gear blank (labeled as Specimen 0 #). After rough grinding, fine grinding, polishing, etching with 4% nitric acid alcohol, the ferrite grain size of the specimen was observed by optical microscope.

(2) Austenite grain size comparison: Two specimens were taken from the Specimen 0 #, labeled as Specimen 1 # and Specimen 2 #. Specimen 1# was heated to 860 °C for 1 h, then quenched in water. Specimen 2 # was annealed firstly (heated to 850 °C for 6 h, cooled to room temperature in the furnace), and then treated in accordance with the Specimen 1# processing. The austenite grain size of the specimens was observed by optical microscope after polishing and etching with a new grain corrosive at 75 °C~80 °C for 13 min.

(3) Carburized layer comparison: Two specimens were continued to take from the Specimen 0 #, labeled as Specimen 3 # and Specimen 4 #. Specimen 3 # was treated as the procedure: carburized in a box-type furnace in accordance with the procedure show as the Figure 1, then tempered at 180 °C for 2 h. Specimen 4 # was annealed as the Specimen 2 #, grinded off the surface oxidized layer, and then treated as the Specimen 3 #. The case hardening, depth and microstructure of the carburized layer of the two specimens were measured.

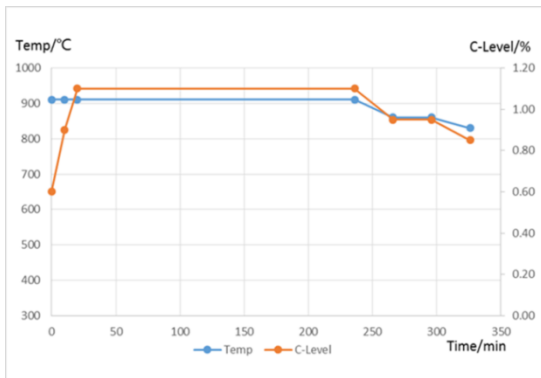


Figure 1 Carburizing process of the specimens

3 Results and Discussion

3.1 Effect of annealing on ferrite grain refining

As shown in Figure 2, after high-temperature heated, the microstructure of the specimen was a typical overheated structure. The grain boundaries tended to be significantly coarse and the grains grew up significantly. The minimum diameter of the ferrite grain was 100 μm and the maximum diameter was 450 μm , the average diameter was 210 μm , the grade of the average grain size was 1.5. After annealing, the ferrite grain size was obviously refined, and the average grain diameter was 25 μm with an average grain size of Grade 7.5 (Figure 3).



Figure 2 Ferrite grain size of specimen 0 # X100



Figure 3 Ferrite grain size of specimen 2 # after annealing X100

As the specimen was insulated above Ac3

temperature, recrystallization occurs during the heat treatment of a deformed material and the grain structure is reconstruction [2]. At first the generation of small new grains is observed. The original coarse grains were re-austenitizing and tended to fine austenite grains in recrystallization process. It can be obtained fine grain in the subsequent cooling [3].

3.2 Effect of heat treatment regime on austenite grain size

Compared Figure 2 with Figure 4a), it can be seen that there was a huge difference between ferrite grain size and austenite grain size for the inherent fine grain steels. The ferrite grain size for the gear blank was only 1.5 while the austenite grain size could reach 7.5.

Therefore, for the forgings which need quenching and tempering or gas carburizing, the evaluation of grain size should be based on the austenite grain size rather than ferrite grain size. This is because that the estimation of grain size base on ferrite grain size is highly misleading, as there may be a phenomenon that ferrite grains grow up while austenite grains do not truly grow. In addition, coarse ferrite grains have obvious inheritance tendency. Parts with coarse ferrite grain size may cause mixed grains during subsequent quenching or gas carburizing. As shown in Figure 2 and Figure 4, the ferrite grains were obviously refined after annealing treatment, and correspondingly, the austenite grain size became significantly more uniform after quenching. Therefore, for parts with coarse ferrite grains, annealing is still necessary to refine the grains and prevent the occurrence of mixed grains.

In addition, it is generally believed that the higher the heating temperature, the larger the grain size. Although the carburizing temperature was 920 $^{\circ}\text{C}$ and the quenching temperature was 860 $^{\circ}\text{C}$, there was no significant difference in grain size between the two specimens.

It is because the Ti element is added to 20CrMnTiH3, which forms TiC or Ti (C/N) second phase particles in the steel to pin austenite grain boundaries and prevent grain growth [4]. Through EPMA, Yuxuan Shi et al. [5] confirmed that the second phase particles TiN with diameter of 3-4 μm were separate out in 20CrMnTiH3. According to Zener's theory, the relationship between grain radius R, second phase particle radius r, second phase particle volume percentage f and grain boundary angle θ satisfies the following conditions [5]:

$$R = \frac{4r}{3f(1+\cos\theta)} \quad (1)$$

From equation (1), it can be seen that when a significant amount of second phase particles with a dispersed and uniformly distributed state separated out, they can prevent the austenite grains growth.

Based on the above experimental results, it can be concluded that annealing treatment can effectively prevent the structural heredity of the ferrite grains growth. This is because annealing treatment is beneficial

for the precipitation of second phase particles [6-7]. The second phase particles can be pinned around grain boundaries, hindering grain growth and facilitating the formation of uniform and fine grains. Additionally, after annealing, an equilibrium microstructure is formed, and during the subsequent quenching process, the equilibrium microstructure is more likely to form a state of uniform and fine grains distribution [7].

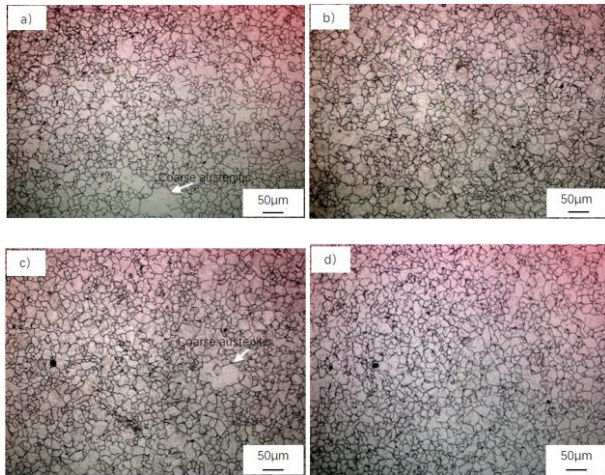


Figure 4 The austenite grain size of the specimens

a) Specimen 1 #: quenched; b) Specimen 2 #: annealed then quenched; c) Specimen 3 #: gas carburized; d) Specimen 4 #: annealed then gas carburized

Table 2 Austenite grain size of specimens under different heat treatment process

| Specimen No. | Heat treatment | Results |
|--------------|---|---|
| 1 # | Specimen with coarse ferrite grains was quenched. | The percentage of fine grain area was 90%, and the average austenite grain size can reach Grade 7.5. Some individual grains can reach 100 µm, the grain size reached Grade 3.5. |
| 2 # | Specimen with coarse ferrite grains was annealed then quenched. | The austenite grains were significantly homogenized, the mixed grains were basically eliminated, and the average grain size can reach Grade 7.5. |
| 3 # | Specimen with coarse ferrite grains was gas carburized. | There was no significant difference in austenite grain size from Specimen 1 #. |
| 4 # | Specimen with coarse ferrite grains was annealed then gas carburized. | There was no significant difference in austenite grain size from Specimen 2 #. |

3.3 Effect of grain size on hardness and intergranular oxidation of gas carburizing parts

The hardness and intergranular oxidation of Specimen 3 # and 4 # with gas carburizing were measured. It can be found that there was no significant difference between the two specimens in the main technical indicators of gas carburizing, including microhardness gradient, effective case hardening depth (The effective case hardening depth is defined as the distance perpendicular to the surface over which a hardness equivalent to 509 HV1 or greater is maintained in the hardened case.), and intergranular oxidation. Therefore, it can be concluded that the ferrite grain size has no obvious effect on hardness and intergranular oxidation of gas carburizing (the ferrite grain size of Specimen 3 # refers to Specimen 0 #, and the ferrite grain size of Specimen 4 # refers to Specimen 2 #).

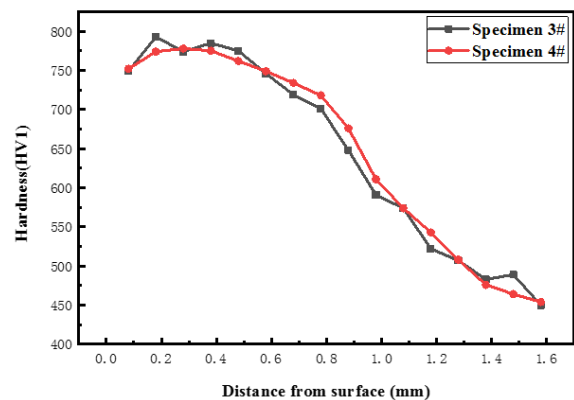


Figure 5 Comparison of microhardness gradient across the carburized case

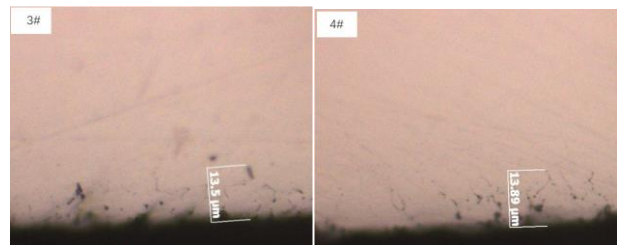


Figure 6 Intergranular oxidation of the specimens

4 Conclusion

(1) In the inherent fine grain steels, there may be significant differences between ferrite grains and austenite grains. For forgings which need to be quenched or gas carburizing, the grain size should be evaluated based on the austenite grain size.

(2) Parts with coarse ferrite grain size may exhibit mixed grains after quenching. However, after annealing treatment, the coarse ferrite grains can be refined and homogenized to avoid mixed grain size during quenching.

(3) The ferrite grain size has no significant effect on

the main technical indicators of gas carburizing, such as microhardness gradient, effective case hardening depth and intergranular oxidation.

Author Contributions: Wangzhan Fan and Weimin Gui conceived and designed the experiments; Youfeng Chen performed the experiments; Weimin Gui analyzed the data. Wangzhan Fan and Weimin Gui wrote the paper.

Conflict of Interest: The authors declare that there is no conflict of interest regarding the publication of this paper.

Acknowledgments: The authors gratefully acknowledge support from the Shaanxi Innovation Talent Promotion Plan-Youth Science and Technology New Star Project (Talent). Project No.:2023KJXX-121.

References

- [1] Dong xu, Cheng Ji, Hongyang Zhao, et al. A new study on the growth behavior of austenite grains during heating process[J]. Scientific Reports, 2017,7:3968.
- [2] G. Gottstein Recovery, Recrystallization, Grain Growth. In: Physical Foundations of Materials Science [M]. Springer: Berlin, Heidelberg, Germany, 2004.
- [3] Yanjin Meng, Xin Guan. Metallurgy and Heat Treatment [M]. Metallurgical Industry Press: Beijing, China, 2008.
- [4] Xiangwei Kong, Kefeng Wang, Zaiyong Lin, et al. Effect of cold deformation on the mixed grain of 20CrMnTi carburized grains and process improvement[J]. Special Steel Technology, 2022,28 (110):24-26.
- [5] Yuxuan Shi, Yujie Ma, Haiyang li, et al. Research on precipitation behavior of nanoscale second phase in carburized gear steels[J]. Modern transportation and metallurgical materials, 2022,11,2 (6):75-80.
- [6] Haihua Wang, Fengyuan Sun, Li Zaiyong, et al. The effect of spheroidization annealing on the carburized grain size of 20Cr gear steel for cold precision forging[J]. Special Steel Technology, 2022,28 (113):37-40.
- [7] Liang Xu, Tao Li, Yongqiang Ma, et al. The effect of annealing process on the grain size of high-temperature bearing steel M50 steel[J]. Special Steel, 2022,43 (6):50-53.

High Temperature Rheological Performance of Graphene Modified Rubber Asphalt

Heyuan GUO^{1*}, Chunhua LI¹, Xin ZHAO¹, Yinghua YUAN¹, Shaoqi TANG¹, Yongjun MENG²

1. GuangXi Vocational College of Safety Engineering, Nanning, Guangxi, 530004, China

2. College of Civil Engineering and Architecture, Guangxi University, Nanning, Guangxi, 530004, China

*Corresponding Author: Heyuan GUO, E-mail: 1020455787@qq.com

Abstract

To elucidate the high temperature rheological capability of graphene modified rubber asphalt, three contents of graphene and crumb rubber were prepared by a combination of mechanical agitation and high speed shearing machine, then used dynamic shear rheological test (DSR) and multiple stress creep recovery (MSCR) tests to evaluate. The hardness and softening point with rotational viscosity of samples raised with the addition of graphene, especially the addition of 0.04%. Dynamic shear rheological test revealed that the dynamic shear modulus G^* , rutting factor $G^*/\sin \delta$, and zero shear viscosity (ZSV) of graphene-modified rubber asphalt were greatly influenced along with graphene-increased, on the contrary, phase angle δ which characterize the viscoelastic ratio of asphalt decreased. Multiple stress creep recovery (MSCR) tests showed that the graphene-enhanced rubber asphalt had high-temperature stability through non-recoverable creep compliance (Jnr). Based on these findings, graphene-modified rubber asphalt binders with the addition of 0.04% graphene had good viscoelastic properties as well as high temperature rutting resistance performance. In the meantime, $G^*/\sin \delta$, ZSV, and Jnr100, Jnr3200 have good correlation, which can reveal the excellent high-temperature stability performance of asphalt.

Keywords: Graphene; High Temperature rheological properties; MSCR; Zero shear viscosity; Rutting

1 Introduction

Rutting is caused by the accumulation of irreversible and permanent deformation for the repeated heavy wheel loadings on the various pavement layers under High-temperature especially, it is one kind of the main damaged of pavement at present. The deformation of rutting is a serious safety hazard to vehicles because hydroplaning can occur in the presence of rutting in rainy weather, setting off serious traffic accidents, and it has been taken into independent detection index of highway technical conditions account. Therefore, asphalt pavement designs and constructions are the most important to prevent the occurrence of rutting deformation problems^[1-2]. The structure stability of asphalt pavement is correlate to the normal use of transportation, and the use of high-quality modified asphalt is one of the key measures to solve the problem of pavement stability, so the development of modified asphalt with excellent performance has important practical significance for the construction of asphalt pavement^[3-5].

Multiple stress creep recovery (MSCR) tests

provide a reasonable basis for construction of high temperature^[6-7], which in a tropical climates and repeated heavy wheel loadings on asphalt pavement, therefore, MSCR is used to evaluate the rutting resistance of asphalt under different stress levels, which characterized by non-recoverable creep compliance Jnr^[8]. Dynamic shear rheology test (DSR) can overcome limitations when measures asphalt binders, rheological properties in a wide scale of temperatures and frequency, based on rheological in many previous studies, the rutting resistance can be used to show the high temperature performance of asphalt pavement^[9-10].

Graphene is a kind of nanomaterial with high-tech and wide application potential, it has been used as an asphalt modifier in practical engineering for its excellent properties^[11]. Many studies^[12-14] show that the additive of graphene enhances the miscibility of modifiers in asphalt binders, increases its high temperature performance of modified asphalt with elasticity and rutting resistance properties. However, there are few studies on the dynamic rheological properties of graphene-modified asphalt, so this paper conducts research on it

In this paper, the high temperature rheological performance of graphene modified rubber asphalt was evaluated using dynamic temperature, frequency scanning and MSCR tests by dynamic shear rheometer, encouraging to the practical engineering application of graphene-modified rubber asphalt.

2 Materials and Methods

2.1 Materials

The base asphalt used in this study is Maoming AH-70. The crumb rubber powders with 40 mesh with a measured density is 1.12g/cm^3 and there is no apparent impurity and it is provided by Changzhou Jingcheng Chemical Co Ltd, China. Graphene is a single-layer graphene (SSA: $50\text{-}200\text{ m}^2/\text{g}$, carbon content is 98%) which is purchased from Shenzhen Turing Evolution Technology Co., Ltd, and the relevant technical indicators of graphene are shown in Table 1:

Table 1 Graphene-related parameters

| Test metrics | Unit | Technical requirements | Result |
|-----------------------|-----------------------|------------------------|--------|
| Bulk density | g/ml | 0.01-0.02 | 0.013 |
| Carbon content | % | — | 98 |
| Specific surface area | m^2/g | 50-200 | 185 |
| water content | % | <2 | 1.3 |
| Monolayer rate | % | >80 | 95 |

2.2 Preparation of graphene modified rubber asphalt binders

The contents of graphene (0%,0.02%,0.04% of original asphalt) modified rubber asphalt binders were prepared by glass rod and high shear mixer to achieve homogenous dispersion of the graphene and rubber in asphalt binders, and the preparation method followed: The base asphalt was heated to the melting flow state in an oven under $135\text{ }^\circ\text{C}$ and the weight of 300 g was melted into a container, a layer of the asbestos net is laid on the heating furnace. The melting asphalt container was heated to keep the glass bar stirred continuously and the temperature of asphalt was recorded with a thermometer at any time. Keep the asphalt temperature $175\text{ }^\circ\text{C}$ and stir for 10 minutes. The crumb rubber powder and graphene were prepared in advance then mixed into the asphalt and stirred successively until all the modifiers were immersed in the asphalt. Then a high-speed shearing machine was used to rotate for 1 hour at a speed of 5000r/min, then the mixture was kept in static condition for 1.5h below $175\text{ }^\circ\text{C}$. The preparation process of graphene modified rubber asphalt binders is illustrated by a flowchart as shown in Figure 1.

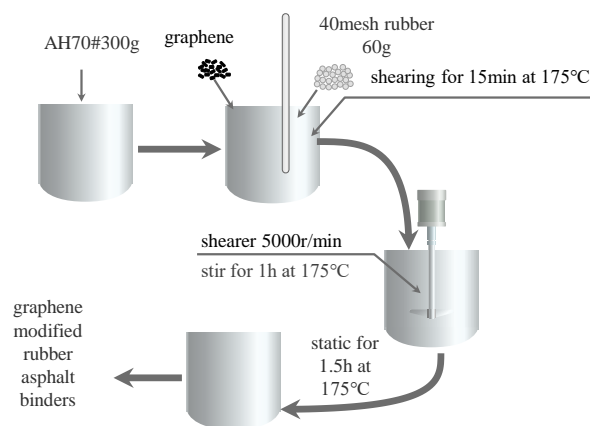


Figure 1 The preparation process of graphene-modified rubber asphalt binders

2.3 Experimental Methods

2.3.1 Physical properties tests

Penetration, softening point, and rotational viscosity are used to be the three main index to value high temperature performance of asphalt binders, which followed the standards of JTG E20-2011 T0604-2011, T0604-2011, and T0625-2011method.

2.3.2 Dynamic temperature sweep test

DSR test of graphene-modified rubber asphalt was carried out with Bohlin CVOR-ADS dynamic shear rheometer which produced by Malvern Instrument Company. The strain is controlled by 2% with a fixed frequency at 10rad/s. The dynamic temperature of graphene-modified rubber asphalt was obtained by temperature sweep at $46\text{-}82\text{ }^\circ\text{C}$ (with an interval of $6\text{ }^\circ\text{C}$). Rutting factor ($G^*/\text{Sin } \delta$), Phase angle, and Dynamic complex modulus of samples were measured under the linear viscoelastic region of asphalt binders.

2.3.3 Dynamic frequency sweep test

To analyze the performance of high temperature viscoelasticity parameters of graphene-modified rubber asphalt, the Dynamic frequency sweep test selected the temperature at $64\text{ }^\circ\text{C}$ as data analysis basis, the frequency was set to $0.1\text{Hz}\sim 10\text{Hz}$, and the strain was controlled to 2%.

2.3.4 Multiple stress creep restoration test (MSCR)

THE MSCR test is carried out through the dynamic shear rheometer, and stress levels are fixed in 100Pa , 3200Pa at $82\text{ }^\circ\text{C}$. One second shear creep load is applied on the sample, following by nine-second recovery, and then ten cycles of creep and recovery were conducted under the shear load.

3 Results and Discussions

3.1 Physical properties tests

Physical property tests which consisted of penetration, softening point, and viscosity at $135\text{ }^\circ\text{C}$ [15-16]

were conducted on three contents of graphene-modified rubber asphalt binders according to JTG E20-2011. The test results are shown in Table 2:

Table 2 Physical properties of three contents of graphene-modified rubber asphalt binders

| Different dosages of graphene | Penetration 25°C (0.1mm) | Softening point (°C) | 135°C Rotational viscosity (Pa·S) |
|-------------------------------|--------------------------|----------------------|-----------------------------------|
| 0% | 43.1 | 69.3 | 7.39 |
| 0.02% | 44.5 | 79.4 | 7.46 |
| 0.04% | 41.2 | 82.4 | 9.89 |

The change of viscosity owing to graphene addition in the rubber asphalt (135°C) is shown in Table 1. It can be found that the viscosity of rubber asphalt with graphene is significantly higher than that of rubber asphalt. It can be concluded that the addition of graphene increases the viscosity of rubber asphalt and enhance the resistance of rubber asphalt to external forces to a certain extent. Obviously the viscosity test showed that graphene modified rubber asphalt has better rutting resistance, excessive viscosity will make asphalt consume more energy during the pumping and mixing, and emitting more greenhouse gases, which is not conducive to environmental protection. In the softening point test, the joining of graphene can improve the softening point and the high temperature stability, comparing to the rubber modified asphalt in the certain extent [17]. Penetration is an important index to evaluate the physical properties of asphalt. In this test, when graphene content is 0.04%, the hardness of modified asphalt was higher, which indicated that it was stable at high temperatures.

3.2 Dynamic temperature sweep test

Dynamic shear rheometer is a basic test instrument of viscoelastic materials. In the pavement performance specification of asphalt, SHRP pointed out that in the process of strain control, the swing plate rotates at specified frequency to complete a specified period, and the same time ,required torque, shear stress, shear strain, and phase angle are measured [18]. The shear stress S , shear strain D , dynamic complex modulus G^* , and phase angle of asphalt specimens are calculated as follows:

$$S = \frac{2T}{\pi r^3} \quad (1)$$

$$D = \frac{\theta r}{h} \quad (2)$$

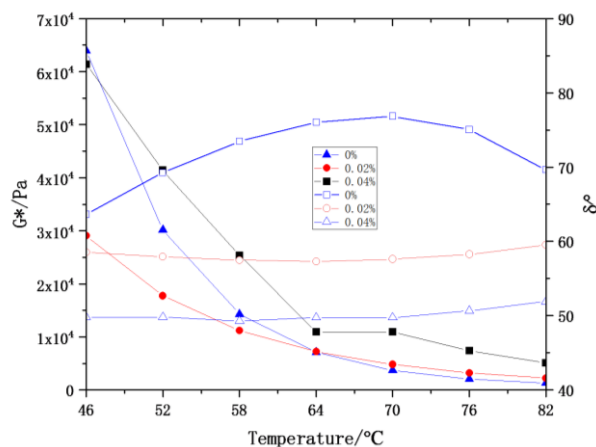
$$G^* = \frac{S_{max} - S_{min}}{D_{max} - D_{min}} \quad (3)$$

$$\delta = 2\pi f \cdot \Delta t \quad (4)$$

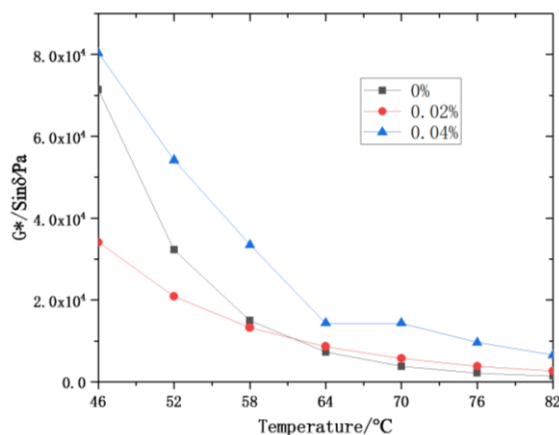
In the formula, T is the maximum torque; R is the radius of the swing plate (12.5mm), h is the height of the specimen (1mm); θ is the rotation angle of the swing plate; S_{max} , S_{min} , D_{max} , D_{min} stands in for the maximum

or minimum shear stress and strain that the specimen bears; and t is the lag time.

There is little doubt about that performances of pavement mainly depending on the viscoelastic and mechanical behavior of asphalt. Until now, the complex modulus G^* , phase angle δ , and rutting factor $G^*/\sin \delta$ of three modified asphalt binders at different temperatures were measured by dynamic shear rheological test to characterize the high temperature performance [19-20]. The results of G^* , δ and $G^*/\sin \delta$ of modified asphalts with temperature is shown in Figure 2:



(a) Complex modulus -temperature- phase angle relationship of different modified asphalt



(b) Rutting factor -temperature relationship of different modified asphalt

Figure 2 The result of dynamic temperature sweep test.

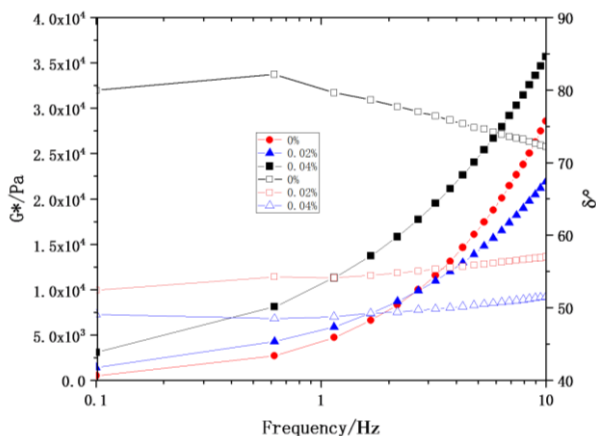
In terms of the research of SHRP, the higher temperature, the anti-rutting performance of asphalt worse, it is well accepted that improving the anti-rutting performance of asphalt is very important [22]. Figure 2(a) showed that the complex modulus G^* , rutting factor $G^*/\sin \delta$ are obviously related to temperature. With the increasing of temperature, the rutting factor $G^*/\sin \delta$ decreases gradually. At relatively low temperature, rubber asphalt with 0.04% graphene content is larger than rubber asphalt with 0.02%, 0% graphene addition. After the temperature is higher than 64°C, the addition of

graphene enhance Dynamic complex modulus G^* , Rutting factor $G^*/\sin \delta$ of rubber asphalt. When the $G^*/\sin \delta$ bigger, the permanent deformation of asphalt binder decrease due to energy dissipation. It showed that graphene-modified rubber asphalt binders have better rutting resistance and stability at high temperatures [23].

Phase angle δ can be used to characterize the viscoelasticity of asphalt [24]. In Fig 2, it is obvious that the fluctuation of phase angle of graphene modified rubber asphalt is gentle with the increase of temperature, and the addition of graphene reduces the phase angle with rubber modified asphalt, which indicates that the modified asphalt binders have good resilience.

3.3 Dynamic frequency sweep test

The loading mode of dynamic frequency sweep following the time-temperature equivalence principle is used to ensure the test conditions and samples meet the linear viscoelastic theory at the same temperature [25]. The changes in dynamic complex modulus and phase angle of modified asphalt were observed at different frequencies. The experimental results are shown in Figure 3:



(c)Complex modulus -frequency- phase angle relationship of different modified asphalt

Figure 3 The results of the dynamic frequency sweep test

The results of dynamic frequency sweep test showed that the complex modulus of modified asphalt increases gradually with the frequency raising, and the dynamic complex modulus of graphene content of 0.04% showed obvious advantages. From the changed of phase angle, the phase angle of graphene modified asphalt binders increase to a certain extent with the frequency raising, which shows that the viscoelastic component of graphene modified asphalt increased and the elastic component decreased gradually. However, compared with rubber modified asphalt, the elastic property of graphene modified asphalt binders is larger, which indicated that graphene modified asphalt resisted external force deformation at high temperatures.

Correlation studies have proclaimed that ZSV can

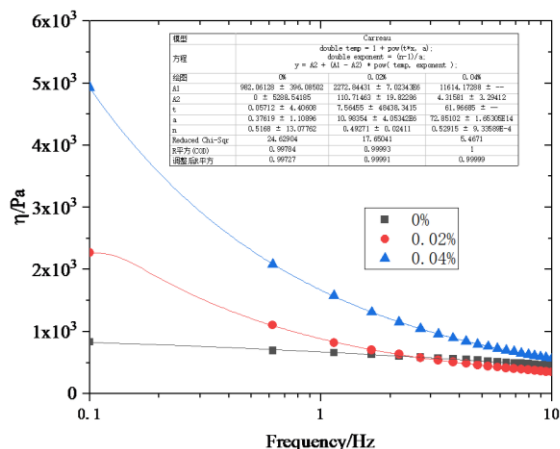
be used as a key index of high temperature performance of asphalt [26-27]. ZSV refers to the viscosities directly measured or calculated at a certain temperature when the shear rate reach or approaches zero, so it can be used to characterize the viscous performance of materials, it is an inherent property of materials, also known as absolute viscosity [28]. Rutting deformation at high temperatures is a slow process, so it is reasonable to use zero shear viscosity be a high temperature performance evaluation of graphene-modified rubber asphalt binders with different content. ZSV can be evaluated by dynamic frequency loading test. In this paper, the Zero shear viscosity of modified asphalt at 64°C was predicted by using Carreau, Cross, and other related models. The Carreau and Cross equations were fitted as follows:

$$\eta_a = \eta_{\infty} + (\eta_0 - \eta_{\infty}) [1 + (\lambda D)^2]^{-\frac{C-1}{2}} \quad (5)$$

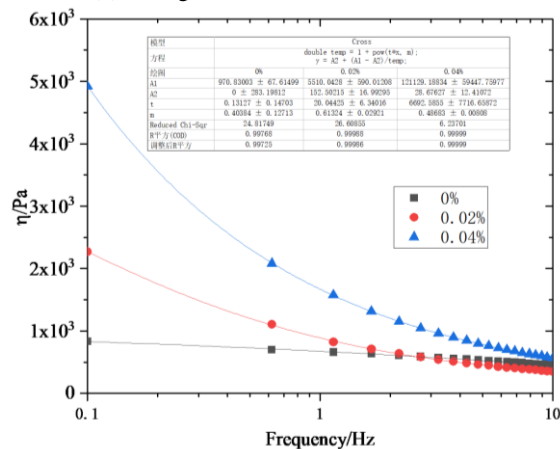
$$\eta_a = \eta_{\infty} + \frac{\eta_0 - \eta_{\infty}}{1 + (k^* D)^P} \quad (6)$$

In the above formulae, D is the shear rate, when $D \rightarrow 0$, there is $\eta_a \rightarrow \eta_0$, which is zero shear viscosity, when $D \rightarrow \infty$, $\eta_a \rightarrow \eta_{\infty}$, shear viscosity, that is, infinite shear viscosity.

According to the fitting results of the experiment, as shown in Figure 4:



(d) Fitting curves based on the carreau model



(e) Fitting curves based on Cross model

Figure 4 Fitting results of zero shear viscosity

Figure 4 shows that with the frequency raising, the complex viscosity of the three different modified asphalts decreases gradually, and there are obvious differences, it can be concluded that this is because of the addition of graphene enhanced viscosity with modified asphalt. Among them, when the content of graphene reach 0.04%, the complex viscosity is increasing markedly, it can be seen from this graphene improved the viscosity with the modified asphalt to a certain extent. ZSV of modified asphalt was obtained by two fitting methods. The calculation table is as follows: Table 3 and Table 4.

Table 3 Carreau fitting parameter results

| Different dosages of graphene | η_0 | Correlation coefficient |
|-------------------------------|----------|-------------------------|
| 0% | 982.1 | 0.99 |
| 0.02% | 2272.8 | 0.99 |
| 0.04% | 11531.3 | 1 |

Table 4 Cross fitting parameter results

| Different dosages of graphene | η_0 | Correlation coefficient |
|-------------------------------|----------|-------------------------|
| 0% | 970.8 | 0.99 |
| 0.02% | 5519.6 | 0.99 |
| 0.04% | 121878.8 | 1 |

Table 3 and 4 show that with the addition of graphene, the ZSV of rubber modified asphalt increase gradually. Moreover, the Zero shear viscosity of graphene modified rubber asphalt with the dosage of 0.04% graphene content was obviously higher than that of the other two additions. The result shows that the rutting resistance of asphalt is obviously enhanced with the addition of graphene, which was beneficial to the high-temperature performance remarkably which had a good correlation with the rutting factor.

3.4 Multiple stress creep recovery (MSCR) tests

MSCR uses the delayed elastic recovery performance of asphalt under applied stress levels to evaluate the high temperature performance of asphalt, and the cumulative strain has a good correlation with the high temperature performance of the mixture [29-30]. Compared to the $G^*/\sin \delta$ of sinusoidal loading pattern, asphalt will produce creep compliance under stress. After stress is removed, some of creep compliance will be recovered while non-recoverable creep compliance will accumulate to the next load-deformation accumulation, which is the special feature of viscoelastic materials [31]. The pavement under repeated loading and unloading of vehicle load is also a process of cumulative deformation, so the MSCR can simulate the asphalt pavement strain accumulation process truly and accurately. Different from the traditional PG grading requirements, MSCR reflects the cumulative deformation of asphalt under

repeat loading and unloading conditions, and the loading pattern is not affected by asphalt deformation [32].

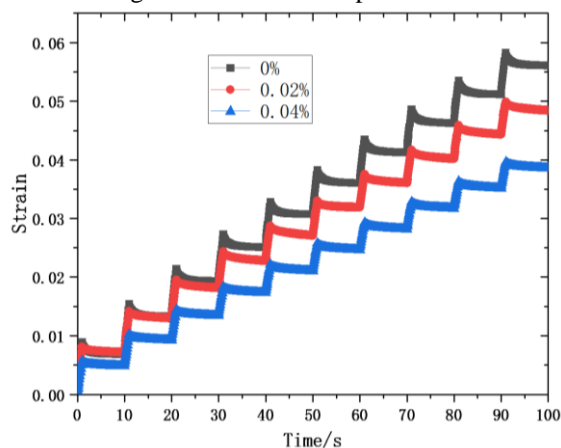
J_{nr} and $J_{nr-diff}$ under different levels of stress are calculated according to the strain collected. The calculation methods are as follows:

$$J_{nr} = \frac{\varepsilon_r - \varepsilon_0}{\delta} \times 100\% \quad (7)$$

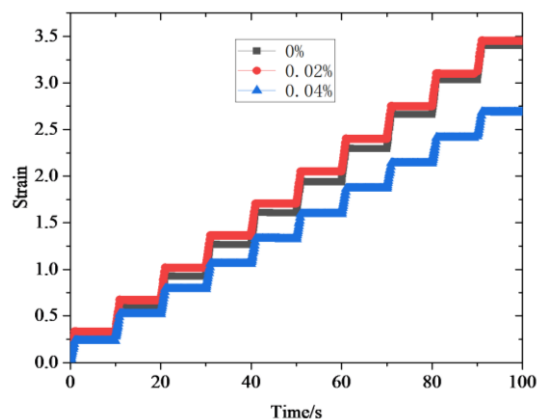
$$J_{nr-diff} = \frac{J_{nr(3200Pa)} - J_{nr(100Pa)}}{J_{nr(3200Pa)}} \times 100\% \quad (8)$$

Where the ε_0 and ε_r represent the initial deformation and residual deformation after 9s Restoration, the “ δ ” represent shear stress, J_{nr} represents non-recoverable creep compliance, while the $J_{nr-diff}$ represents the rate of increase in J_{nr} value when the stress changes from 100Pa to 3200Pa.

Figure 5 show the MSCR test results of three different kinds of graphene modified rubber asphalt under two stress levels. The horizontal ordinate is the whole time of the test, and the longitudinal coordinate is the strain change of the modified asphalt.



(f) Time-strain relationship of different modified asphalt (100Pa)



(g) Time-strain relationship of different modified asphalt (3200Pa)

Figure 5 The results of multiple stress creep recovery (MSCR) tests

According to Figure 5, non-recoverable compliance

values at 100Pa and 3200Pa stress levels can be obtained as shown in Table 5.

Table 5 100 Pa and 3200 Pa stress levels for non-recoverable compliance values

| Different dosages of graphene | J_{nr100} (KPa) | J_{nr3200} (KPa) | $J_{nr-diff}$ (%) |
|-------------------------------|-------------------|--------------------|-------------------|
| 0% | 0.56 | 1.06 | 47.2 |
| 0.02% | 0.48 | 1.08 | 55.1 |
| 0.04% | 0.38 | 0.84 | 54 |

The results of the MSCR test show that J_{nr} at 3200Pa is larger than that at 100Pa, which indicated that with the creep load level increasing, the asphalt maximum strain level also increase. This is mainly due to the higher permanent deformation and lower percent recovery during the creep loading level increase Under two stress levels, asphalt with a graphene content of 0.04% has a smaller J_{nr} . It could be seen that the content of graphene decrease the viscous deformation of asphalt and had better high temperature deformation resistance, which had a good correlation with the rutting factor and zero shear viscosity mentioned above.

Compared with ordinary rubber asphalt, the rate of change of non-recoverable creep stress with the time of graphene-modified rubber asphalt $J_{nr-diff}$ improved with the increase of graphene addition, shows that although the higher content of graphene, it had better high-temperature deformation resistance, but it's viscous deformation was more obvious since the shear stress.

4 Conclusion

40 mesh crumb rubber powder and single-layer graphene were used as asphalt modifiers in this study, the high temperature performances of different addition of graphene modified rubber asphalt were characterized by using DSR and MSCR, and variance analysis was verified feasibility through J_{nr} and $J_{nr-diff}$ to evaluate high-temperature performance of graphene modified rubber asphalt. Based on this limited laboratory survey, the following conclusions are shown:

(1) According to the results of the dynamic temperature sweep test, adding graphene to modified rubber asphalt leads to the increase of rutting factor, which improve the high temperature performance of asphalt lead to a higher working temperature range.

(2) In the DSR test, it was obvious that the addition of graphene made the modified rubber asphalt have better deformation resistance and elastic recovery ability at high temperatures. With the temperature raising, the rutting resistance of rubber asphalt with 0.04% addition of graphene was the best. Zero shear viscosity (ZSV) of modified asphalt is predicted by fitting Carreau and Cross models. It was found that the addition of graphene significantly improved the rutting resistance of asphalt and the high temperature performance of asphalt.

(3) The strain response and delayed elasticity of rubber asphalt and graphene modified rubber asphalt were observed by the MSCR test. The results show that the high temperature performance of graphene modified rubber asphalt is greatly affected by the stress level. According to the non-recoverable creep compliance (J_{nr}) obtained from the MSCR test, it could be found that the rutting resistance of graphene modified rubber asphalt is significantly improved compared with rubber asphalt. Generally speaking, it shows that the positive effect of graphene content on permanent deformation is 0.04%.

(4) The process of residual deformation is caused by repeating loading and unloading in multiple stress creep recovery test (MSCR) had a great extent correlation with the process of rutting was caused by vehicle loading at a certain temperature.

For the application of graphene to modified asphalt pavement, relevant demonstration engineering applications have been carried out, but further exploration and research are still needed in the macro and micro properties of graphene-modified asphalt, so as to improve the development requirements of road durability.

References

- [1] Cai LL. Evaluation of High Temperature Performance of Modified Asphalt Binder by Multiple Stress Repetitive Creep Recovery (MSCR) Method[J]. *Petroleum Asphalt*, 2013,27(6):21-24.
- [2] Ren RB, Gen LT, Xu Q. Performance of Reclaimed Rubber-Plastic Modified Asphalt and it's Mixture[J]. *Journal of Building Materials*, 2016,19(6):1092-1096+1110.
- [3] Prabin KA, Dharamveer S, Siva B. Evaluation of rutting, fatigue and moisture damage performance of nanoclay modified asphalt binder[J]. *Construction and Building Materials*, 2016,113:341-350.
- [4] Gilles O, Martin, JV, Menapace A. Rutting and Moisture Resistance of Asphalt Mixtures Containing Polymer and Polyphosphoric Acid Modified Bitumen[J]. *Road Materials and Pavement Design*, 2004,5(3):323-354.
- [5] Mohammad R, Ellie HF, MASCE PH. Rutting Characteristics of Styrene-Ethylene/Propylene-Styrene Polymer Modified Asphalt[J]. *Journal of Materials in Civil Engineers*, 2015,27(4):4014154.
- [6] Qiao XB, Li XM, Wei DB. Research on Rubber/SBS Modified Asphalt by MSCR Test[J]. *Advanced Materials Research*, 2012,557-559:1066-1069.
- [7] Xu JG, Han B, Wang YL. Research on Rutting Resistance of Asphalt Pavement[J]. *Road Machinery & Construction Mechanization*, 2011,28(01):59-62.
- [8] Kataware A V, Singh D. A study on rutting susceptibility of asphalt binders at high stresses using MSCR test[J]. *Innovative Infrastructure Solutions*, 2017,2:4.
- [9] Wang JS, Wu SP, Han J. Rheological properties of asphalt modified by supramolecular UV resistant material-LDHs[J]. *Journal of Wuhan University of Technology-Mater*,

- 2012,27(4):805-809.
- [10] Yang E, Zhang XN. The Study of High Temperature Performance of Asphalt Modified by Trinidad Lake Asphalt[J]. *Advanced Materials Research*, 2013,831:387-392.
- [11] Shen PK, Liu H. 3D Graphene is Expected to Crack Application Problems[J]. *Qinghai Science and Technology*, 2016(1):82-83.
- [12] Moreno-Navarroa F, Sol-Sancheza M, Gámiz F. Mechanical and thermal properties of graphene modified asphalt binders[J]. *Construction and Building Materials*, 2018,180:265-274.
- [13] Liu KF, Zhang K, Shi XM. Performance evaluation and modification mechanism analysis of asphalt binders modified by graphene oxide[J]. *Construction and Building Materials*, 2018,163:880-889.
- [14] Huang JY, Ye QS. Experimental Study on Rheological Properties of SBS-graphene Composite Modified Asphalt[J]. *Transportation Science & Technology*, 2018(1):131-133.
- [15] Cai JX, Yong J, Wan L. Study on Basic Properties and High-Temperature Performance of Rice-Husk-Ash-Modified-Asphalt[J]. *Applied Mechanics and Materials*, 2013,333-335:1889-1894.
- [16] Aliasghar AN, Koorosh N, Mostafa N. High-temperature performance of gilsonite -modified asphalt binder and asphalt concrete[J]. *Petroleum Science and Technology*, 2016,34(21):1783-1789.
- [17] Li F, Li TG, Shi XP. Evaluation on High-temperature Adhesion Performance of Hot-applied Sealant for Asphalt Pavement[J]. *Journal of Wuhan University of Technology (Materials Science Edition)*, 2014,29(6):1237-1241.
- [18] Wang L, Chang CQ. Rheological Evaluation of Polymer Modified Asphalt Binders[J]. *Journal of Wuhan University of Technology (Materials Science Edition)*, 2015,30(4):695-702.
- [19] HAN M Z, LI J, MUHAMMAD Y S. Studies on the secondary modification of SBS modified asphalt by the application of octadecyl amine grafted graphene nanoplatelets as modifier[J]. *Diamond and Related Materials*, 2018,89:140-150.
- [20] Zhang XH. Common Performance Research of Carbon Nano Tube/Rubber Composite Modified Asphalt[J]. *China Municipal Engineering*, 2016(4):80-81,106-107.
- [21] Li X, Jian C, Guo HQ. Microstructure and performance of crumb rubber modified asphalt[J]. *Construction and Building Materials*, 2009,23(12):3586-3590.
- [22] Zhang R, Wang HN, Gao JF. High temperature performance of SBS modified bio-asphalt[J]. *Construction and Building Materials*, 2017,144:99-105.
- [23] Zhou YM, Wei JG, Shi S. Properties of composite-modified asphalt with polyphosphoric acid and rubber powder[J]. *Journal of Chang an University (Natural Science Edition)*, 2018,38(5):9-17.
- [24] Li L, Zhang HL, Chen ZH. Physical and rheological evaluation of aging behaviors of SBS modified asphalt with thermochromic powders[J]. *Construction and Building Materials*, 2018,193:135-141.
- [25] Tan YQ. *Viscoelastic characteristics of asphalt binder and asphalt mixture*[M]. Harbin Institute of Technology Press: Harbin, 2017.
- [26] Meng YJ, Zhang XN, Jia J. Research on zero shear viscosity of asphalt based on different loading modes[J]. *Journal of Traffic and Transportation Engineering*, 2008(4):35-39.
- [27] Erik O, Safwat S. Assessment of ZSV in Asphalt Concrete Using Shear Frequency Sweep[J]. *Testing, Journal of Materials in Civil Engineering*, 2012,24(10):1305-1309.
- [28] Lei Y, Wang HN, Fini EH. Evaluation of the effect of bio-oil on the high-temperature performance of rubber modified asphalt[J]. *Construction and Building Materials*, 2018,191:692-701.
- [29] John D'Angelo. *Guidance on the Use of the MSCR Test with the M320 Specification*[R]. KENTUCKY: Asphalt Institute Technical Advisory Committee, 2010.
- [30] Ali AW, Kim HH, Mazumder M. Multiple Stress Creep Recovery (MSCR) characterization of polymer modified asphalt binder containing wax additives[J]. *International Journal of Pavement Research and Technology*, 2018, S1996681418300063.
- [31] Qiao XB, Li XM, Wei DB. Research on rubber/SBS modified asphalt by MSCR test[J]. *Advanced Materials Research*, 2012,557-559:1066-1069.
- [32] Fang XY, Luo R, Feng GL. Evaluation Index of High Temperature Performance of Rutting Resistant Modified Asphalt[J]. *Journal of Wuhan University of Technology (Transportation Science & Engineering)*, 2017,41(4):618-622.

Research Progress of High Entropy Ceramic Materials

Song WU, Shikai LIU*, Jialin WANG, Bibo HAN, Shaoyi SHEN, Zhigang YU, Zhaobo ZHANG, Xinhua ZHENG

School of Materials Science and Engineering, Henan University of Technology, Zhengzhou, Henan, 450001, China

*Corresponding Author: Shikai LIU, E-mail: Shikai Liu at shikai_liu@haut.edu.cn

Abstract

High-entropy materials (HEMs) have better mechanical, thermal, and electrical properties than traditional materials due to their special "high entropy effect". They can also adjust the performance of high entropy ceramics by adjusting the proportion of raw materials, and have broad application prospects in many fields. This article provides a review of the high entropy effect, preparation methods, and main applications of high entropy ceramic materials, especially exploring relevant research on high entropy perovskite ceramics. It is expected to provide reference for the promotion of scientific research and the development of further large-scale applications of high-entropy ceramic materials.

Keywords: High-entropy ceramic materials; high entropy effect; preparation method; perovskite structure; research prog

1 Introduction

With the rapid development of science and technology, higher requirements are being placed on the performance of materials. For ceramic materials, a single principal component ceramic material can no longer meet the performance requirements under harsh usage conditions. Inspired by the development of high-entropy alloys, scientists have introduced the concept of high-entropy into the field of ceramics. The concept of HEM originates from high entropy alloys (HEAs). In 2004, Ye^[1] innovatively proposed HEAs. This alloy is typically made up of five or more metallic elements in equal or almost equal proportions. It is a single structured solid solution with multiple main elements. Its structure is ordered long-range, but its components are disordered. This new discovery breaks through the traditional design concept of single principal component materials and provides new ideas for the design of new materials. As the concept of high entropy gradually improves in the field of alloys, it is gradually introduced into the field of other materials. In 2015, Rostet al^[2]. at North Carolina State University, one of the pioneers in the field of high entropy in the United States, successfully synthesized $(\text{Mg}_{0.2}\text{Co}_{0.2}\text{Ni}_{0.2}\text{Zn}_{0.2}\text{Cu}_{0.2})\text{O}$. On considering the influence of the configurational entropy on its structure, it was named entropy stable oxide (ESO). After that, researchers at home and abroad have successively studied various high-entropy systems, including fluorite-structured^[3], perovskite-structured^[4], spinel-structured high-entropy oxide ceramics^[5], as well

as non-oxide high-entropy ceramics, such as nitrides^[6], borides, and so on^[7]. Although the research on high-entropy ceramics is hot, it is still in its infancy, and there is still a lot of work to be done.

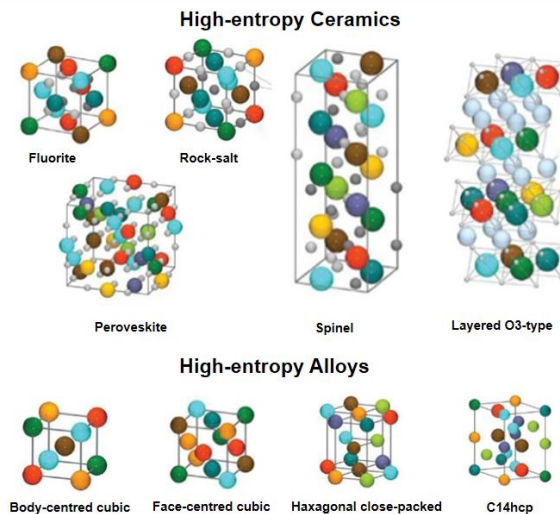


Figure 1 Structure of several high-entropy ceramics and alloys

2 Core Effects of High-entropy Materials

2.1 Thermodynamic high-entropy effects

The "entropy" of high-entropy ceramics is the configuration entropy (ΔS_{mix}), whose relationship with the number of components in the HEMs is shown in

Figure 2 (a). According to Boltzmann's assumptions about the change in entropy and the degree of chaos, the greater the variety of elements [8], the greater the degree of chaos. If the effects of atomic vibrational grouping, electronic grouping, magnetic moment grouping, and other factors are considered at this point, the entropy change of HEMs is greater. Multiple major elements in each high-entropy material can be added in equal or unequal molar ratios, which leaves a wealth of scope for the design of high-entropy materials. The high-entropy effect can be used to explain the formation of HEAs with multiple principal elements as shown in Figure 2(b). On the one hand, the high mixing entropy at high temperature can effectively reduce the Gibbs free energy of the alloy system, thus stabilising the generated single phase; on the other hand, high entropy can reduce the electronegativity difference, inhibit the formation of compounds, and promote the mixing between elements. The solid solution phase in HEA will produce a strong solid solution strengthening effect, which can significantly improve the mechanical properties of the alloy such as strength and hardness [9].

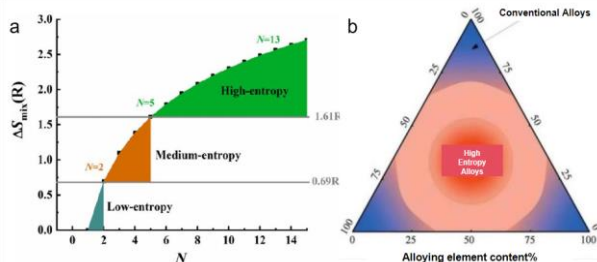


Figure 2 (a) Conformational entropy vs. number of group elements; (b) Relationship between the content of high entropy alloy element [9]

2.2 Effects of lattice distortion of structures

Unlike the lattice distortion of conventional materials [10], the elements in HEMs are numerous and often exist in equal molar ratios, so that all types of atom have the same chance to occupy fixed positions on the lattice. Since the various types of will be randomly distributed in the crystal structure, the different sizes of the atoms and the large difference in chemical bonding will cause more serious lattice distortions within the structure of the high-entropy materials. If the sizes of the atoms are very different, the lattice will not be able to maintain a normal structure because of the high degree of distortion, leading to the generation of amorphous phases.

2.3 Hysteresis-diffusion effects of dynamics

During the alloy material moulding process, the atoms will gradually converge from the chaotic arrangement in the molten state, and after the synergistic coordination and diffusion of the components, there will

be a split phase, leading to easy nuclei formation in the alloys but not easy to grow [11]. In high-entropy alloys, the large difference in atom size, the greater variety of elements, the more complex structure, the slower rate of internal diffusion and phase transitions and therefore the precipitation of nanometer-sized grains, which is not possible in conventional alloys, is often observed. This phenomenon results in HEAs that do not undergo grain growth and recrystallization at elevated temperatures, which has the potential to greatly improve the corrosion resistance of alloyed materials.

2.4 Cocktail effect

For HEMs, the basic properties of different components and the interactions between them can lead to the emergence of more complex properties of high-entropy materials. By changing the amount and type of added components, some of the properties of the material can be regulated, and even new certain properties can appear. The high-entropy effect allows high-entropy ceramics to remain single phase at extreme temperatures, pressures and chemical environments [9]. The kinetic hysteretic diffusion effect allows high entropy ceramics to be synthesized at high temperatures and maintain structural stability at room temperature. The kinetic hysteretic diffusion effect also leads to the formation of amorphous or nanocrystalline structures in high entropy ceramics, which endows them with corrosion-resistant properties. The low amorphous thermal conductivity is related to lattice distortion effects, and, together with the high hardness, it promotes the development of materials for thermal and environmental barrier protection. The lattice distortion induced by many elements of different sizes produces a solid solution strengthening leading to an improvement in their mechanical properties [12], mainly by preventing dislocation motion and modifying and eliminating the lattice slip regime through the resulting nanograin microstructure [13]. The suppression of grain coarsening at high temperatures has also been attributed to lattice distortion (LD) effects, where the distortion of the lattice increases the crystallization energy of the crystals, thus reducing the free energy gained by shrinking the surface area of the grains.

3 Method of Preparation of High-entropy Ceramic Powder

3.1 Solid phase reaction method

The solid-state reaction method often uses mechanical alloying technology to prepare powders, starting from elemental metal or metal ceramic powders. In this process, by using different types of metal ceramic powders and adding alcohol or stearic acid as process control agents, high energy is applied through high-energy ball milling equipment to produce partially

or completely mechanically alloyed high-entropy ceramic powders. Wang et al ^[14], successfully prepared single-phase (Hf, Zr, Ta, Nb, Ti) (C, N) with high entropy using various oxide powders in a flowing nitrogen environment, after high energy ball milling to provide higher energy to the powder, at temperatures above 1400 °C. This powder has a single-crystal cubic structure and high compositional uniformity. As the reaction temperature increases, the grain size of high-entropy carbonitrides increases, with the average particle size increasing from 0.31 to 1.26 μm. In addition, various anions can be introduced through solid-state reactions to adjust the composition and content. For example, amorphous BCN powder can be obtained by mechanically alloying equimolar graphite powder with metal nitrogen boron compounds for 10 h. After 24 h of high-energy ball milling, a nano-high entropy ceramic powder with a face-centered cubic rock salt structure was finally formed.

3.2 Preceramicpolymer pyrolysis

Although the solid phase reaction method is widely used in material preparation, it also has some shortcomings, such as the high reaction temperature, long reaction time, difficulty in accurately controlling the proportion of the product, and easy introduction of impurities during the preparation process ^[15]. To overcome these challenges, researchers have developed a new method for synthesizing ceramics with high entropy under relatively mild conditions, drawing on the strategy of precursor preparation of ceramics. This method includes the use of the sol-gel method and coprecipitation method to realize the mixing of raw materials at the atomic level, thereby reducing the energy required for the synthesis of HEMs. Moreover, sufficient calcination is carried out at relatively low temperatures to remove excess crosslinking agents, precipitants, or solvents, achieving a low-temperature synthesis of high-entropy ceramics. Compared to the atoms in solid powders, the powder prepared by precursor conversion has a significant improvement in atomic diffusion rate, resulting in higher entropy ceramic powders with more uniform composition distribution and more unified crystal structure. The precursor pyrolysis method not only has the advantages of mild reaction conditions, controllable product particle size, and purer products but also faces problems such as low yield, complex process, high equipment requirements, and difficulty in reinterring product particles.

3.2.1 Sol-gel method

The Sol-gel method is a technology that uses compounds containing highly chemically active components as precursors. In this method, the raw materials are mixed uniformly in the liquid phase and undergo hydrolysis and condensation chemical reactions to form a stable transparent sol system in the solution.

With the passage of time, the colloidal particles in the sol gradually polymerize slowly to form a three-dimensional network structure of gel ^[16], which is filled with solvent that has lost its mobility. After drying and sintering solidification processes, materials with molecular to nanoscale substructures were finally prepared. Zhang et al ^[17], successfully prepared (La_{0.2}Y_{0.2}Nd_{0.2}Gd_{0.2}Sr_{0.2}) CrO₃ ceramic powders (La_{0.2}Y_{0.2}Nd_{0.2}Gd_{0.2}Sr_{0.2}) using the sol-gel method. This method not only overcomes the limitation that the 34conventional solid phase method requires high-temperature calcination at more than 1300 °C, but also realizes the fine and uniform distribution of powders and the uniform dispersion of elements.

3.2.2 Coprecipitation method

The coprecipitation method is a technology that adds an appropriate precipitant to the electrolyte solution containing various ions, to initiate the reaction to generate homogeneous precipitates, and then thermally decomposes these precipitates to obtain high-purity nano powder materials. The advantages of this method are twofold. First, it can be directly obtained from nanopowder materials with uniform chemical composition through chemical reaction in solution. Second, the method facilitates the preparation of nanopowder materials with small particle size and uniform distribution. Wang et al ^[18], successfully prepared multi-metal MOF precursors by chemical precipitation method at room temperature, and obtained the general formula through the treatment with high entropy alloy CoNiCuMnAl@C nanocatalysts. This catalyst not only exhibits excellent redox reaction (OER) performance but also exhibits excellent durability.

3.3 Molten salt method

The molten salt method uses various low melting point salts as reaction media to dissolve the reactants in the molten salt for the reaction. Compared to the diffusion rate of atoms in solid-phase powders, the diffusion rate of salt atoms in the molten state at high temperatures is significantly increased, which can significantly shorten the preparation time of powders. After sufficient reaction, the salt substances were dissolved and wash with appropriate solvents to obtain HETMCC powder. This method not only has a simple process and low synthesis temperature, but can also obtain powder with uniform composition. Chu et al ^[19], synthesized nano (Ta_{0.25}Nb_{0.25}Ti_{0.25}V_{0.25}) C with single-phase rock salt structure using four types of metal powders and carbon powders as raw materials and potassium chloride as molten salt medium under first-principles guidance at 1300 °C. The powders exhibited good compositional uniformity.

4 The Application of High Entropy Ceramics

The high entropy effect significantly improves the

mechanical performance of high entropy ceramics (HECs), pushing them beyond the traditional boundaries of mixture rules and theoretical predictions^[20]. This emerging paradigm in material design, coupled with infinite possibilities of component and microstructure combinations, provides HECs with performance characteristics that traditional materials cannot match. The potential applications of this family of materials are extensive, spanning various fields from structure to functionality. Specific applications include ultra-high temperature thermal protection and insulation for hypersonic aircrafts, thermal protection and environmental barrier coatings for engine components^[21], radiation-resistant materials for nuclear facilities^[22], wear-resistant coatings for cutting tools, materials for electromagnetic wave absorption and interference shielding^[23], anodes for rechargeable batteries, catalysts for clean energy and environmental protection, thermoelectric devices, and supercapacitors, as illustrated in Figure 3.

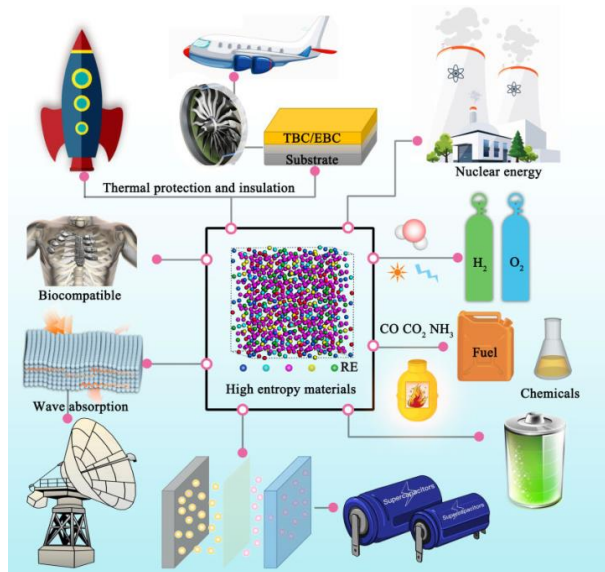


Figure 3 From applications in ultra-high temperature structures to energy and catalytic functional applications

4.1 Supercapacitor

Supercapacitors are currently the world's largest mass-produced double-layer capacitors, mainly divided into carbon-based, metal oxide, and polymer supercapacitors based on electrode materials. Among them, carbon-based supercapacitors are particularly outstanding due to their wide applications, and their performance mostly depends on factors such as the characteristics of carbon materials, the specific surface area of electrode materials, particle size distribution, conductivity, and electrochemical stability. By introducing HEMs into carbon-based electrode materials, it is possible to increase the active sites and surface area, improve the electrochemical stability, and thus achieve higher capacity and current density. Jin et

al. successfully synthesized (CrMoNbVZr) N using a mechanochemical soft urea method, with a specific capacitance between 230 and 54 F/g, significantly better than carbon-coated tin oxide nanofibers (118 F/g) under the same conditions.

4.2 Thermoelectric materials

When disorder is introduced into the material, its thermal conductivity can be effectively reduced^[25]. This reduced lattice thermal conductivity makes high-entropy ceramic semiconductors ideal materials in the field of thermoelectric. Zhang et al^[26]. Successfully prepared a novel high-entropy perovskite-type ceramic $(\text{Ca}_{0.2}\text{Sr}_{0.2}\text{Ba}_{0.2}\text{La}_{0.2}\text{Pb}_{0.2})\text{TiO}_3$ (abbreviated as CSBLP) using the solid-state reaction method. This high-entropy ceramic exhibits both long-range structural order and short-range chemical disorder, with uniformly distributed nanosized grains ranging from 4 to 6 nanometers in its microstructure. Benefiting from the increased configurational entropy, the CSBLP ceramic demonstrates a high Seebeck coefficient ($|S|$ 272 $\mu\text{V}/\text{K}$ at 1073 K) and low thermal conductivity (κ is 1.75 $\text{W}/\text{m}\cdot\text{K}$ at 1073 K) after annealing at 1300 °C. This study demonstrates the feasibility of effectively reducing the thermal conductivity of thermoelectric oxides and improving their thermoelectric performance through the design of high-entropy compositions.

4.3 Catalyst

High-entropy alloys, because of their excellent corrosion resistance, have surpassed traditional transition-metal alloys and find wide applications as electrocatalysts in acidic or alkaline environments. These alloys exhibit good catalytic performance in reactions of oxidation (methanol, ammonia, and carbon monoxide), decomposition (ammonia), and reduction (oxygen). The different atomic bonding in high-entropy ceramics provides outstanding catalytic activity, and by adjusting their unique geometric structure or pore structure to increase surface area, their performance can be further enhanced. Riley et al^[27]. synthesized high-surface-area high-entropy oxides (HEO) $(\text{CeLaPrSmY})\text{O}_{2-y}$ using a sol gel method in the presence of polymer complexing agents, followed by calcination at lower temperatures. This high-entropy ceramic maintains a single-phase structure even at high temperatures and exhibits activity without the need for expensive platinum group metals. Furthermore, Riley et al. also compared the catalytic performance of $(\text{CeLaPrSmY})\text{O}_{2-y}$ synthesized by solid-phase synthesis with that synthesized by the sol-gel method with CeO_2 in the oxidation-reduction reaction of carbon monoxide. The results showed an improvement in the catalytic activity of both HEOs; compared to the solid-state samples, the sol-gel method-prepared HEOs exhibited higher activity because of their larger surface area.

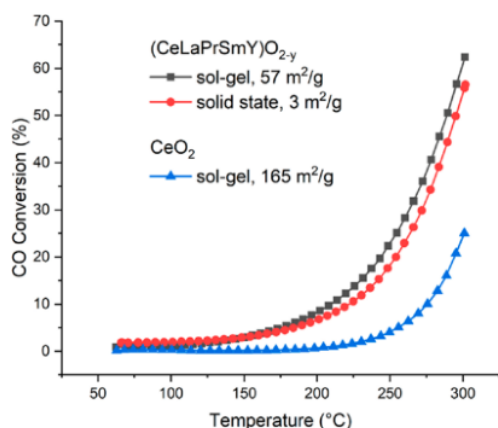


Figure 4 CO oxidation activity of (CeLaPrSmY) O_{2-y} solid and sol gel samples and CeO₂ sol gel samples with the corresponding specific surface area

4.4 Thermoelectric materials

The lower lattice thermal conductivity of HEMs makes it possible for them to be used as semiconductors in thermoelectric devices. In 2018, Roychowdhury et al.^[28] successfully prepared a high entropy selenide (AgBiGe) Se with a single phase rock salt structure in a closed environment using a melting reaction method and studied it using GeSe and AgBiSe₂ as raw materials. The experimental results show that at 677 K, its optimal thermoelectric value ZT reaches the maximum value of 0.45, demonstrating its excellent thermoelectric performance. And at 677 K, the thermal conductivity of the material is 3.8 W/m K, which drops to 0.43 W/m K at 300K.

4.5 Dielectric materials

In high-entropy ceramics, multiple sublattice structures exist, with each structure being occupied by multiple elements. These sub-lattices exhibit not only long-range periodicity, but also their structural distortions affect electronic behavior, dipole response, and band structure. Simultaneously, the random distribution of elements leads to compositional disorder, thereby reducing short-range order. This characteristic makes the dielectric properties of the material easy to manipulate. The dielectric constant, as an indicator of the degree of polarization of dielectric materials in an external electric field, increases with a stronger polarization degree. Zhou et al.^[29] studied the dielectric properties of the high entropy perovskite oxide Ba(Zr_{0.2}Ti_{0.2}Sn_{0.2}Hf_{0.2}Me_{0.2})O₃ (where Me represents Nb⁵⁺ and Ta⁵⁺). They found that within the frequency range of 1 kHz to 1000 kHz, the dielectric constant and dielectric loss decreased slightly with increasing frequency. Within the temperature of 303 K~473 K, this material exhibited good dielectric constant and loss stability at specific frequencies. Specifically, within the frequency range of 1 kHz to 1000 kHz, the dielectric constant of Ba(Zr_{0.2}Ti_{0.2}Sn_{0.2}Hf_{0.2}Me_{0.2})O₃ ranged

approximately 90 ~ 113, while the dielectric loss remained between 120~140.

5 Research Progress in High Entropy Perovskite Ceramics

The basic structure of the perovskite oxides is ABO₃, which is similar to HEA. In this structure, the anionic sublattice is occupied by oxygen elements, and the introduction of different cations into the cationic sublattice will complicate the structure. Its calculation method is:

$$\Delta S_{mix} = -R[(\sum_{i=1}^n c_i \ln c_i)_{cation-site} + (\sum_{i=1}^n c_i \ln c_i)_{anion-site}]$$

n is the number of constituent elements, c_i is the molar fraction of the i-th component, and R is the gas constant. The difference from HEAs is that the unique A and B cation sites in the perovskite structure need to be considered separately. Due to the ability of perovskite structures to accommodate a large number of different cation substitutions, different systems can be constructed by the high entropy of a single cation site or the simultaneous high entropy of two cation sites^[30]. Current research mostly focuses on high-entropy systems with single-cation sites.

Jiang et al.^[31] prepared a high entropy perovskite oxide (HEPO) system for the first time, fixing Sr and Ba at the A site and trying to fix four elements and replace the other four elements at the B site, resulting in a total of 13 high entropy perovskite ceramics at the B site. By analyzing the difference in particle size (& B) and tolerance factor (t), it was found that a t value less than 1.03 is a necessary condition for the formation of a single phase structure. Early research mainly focused on the synthesis methods and structural characterization of HEPOs. Chellali et al.^[32] and Sharma et al.^[33] respectively used atomic probe microscopy (APT) and electron energy loss spectroscopy (EELS) techniques to observe the powders prepared with high entropy perovskite oxide (HEPO) and single crystals, and found that all elements were uniformly distributed at the atomic level. Sakar et al.^[34] successfully synthesized five high entropy perovskite ceramics at sites A and B, as well as a kind of ten-element system. The existence of an entropy stabilization effect in HEPOs was demonstrated through cyclic heat treatment in (5A0.2) MnO₃. Zhong et al.^[35] proposed a new concept through phase diagram calculations, stating that the "high entropy" characteristics of HEPOs involve multiple species such as anions, cations, and defects, and their component concentrations are difficult to directly determine, which is fundamentally different from HEAs.

Afterward, researchers changed their focus from exploring the basic structure of HEPOs to exploring their performance. Zhang et al.^[26] prepared thermoelectric ceramics (Ca_{0.2}Sr_{0.2}Ba_{0.2}La_{0.2}) TiO₃ with low thermal conductivity using phonon engineering techniques.

Thermal conductivity at 1073 K was 2.5 W/(m K), and thermal conductivity was further reduced to 1.75 W/(m K) by introducing Pb at the A site. In the field of dielectric materials, high-entropy A-site perovskite materials have also received widespread attention. Zhong et al. [35] pointed out in their study that the lattice distortion present in high-entropy perovskite oxides of site A significantly affects their antiferroelectric phase transition behavior. Xiong et al. [36] observed that $(\text{Ca}_{0.25}\text{Sr}_{0.25}\text{Ba}_{0.25}\text{Pb}_{0.25})\text{TiO}_3$ ceramics exhibit low loss (tan) within 25~125 °C, The coexistence of long-range ferroelectricity and quasi relaxation behavior. Pu et al. [37] simultaneously found 1.02 J/cm³ in $(\text{Na}_{0.2}\text{Bi}_{0.2}\text{Ba}_{0.2}\text{Sr}_{0.2}\text{Ca}_{0.2})\text{TiO}_3$ ceramics $(\text{Na}_{0.2}\text{Bi}_{0.2}\text{Ba}_{0.2}\text{Sr}_{0.2}\text{Ca}_{0.2})$ The high discharge energy density and the significant adiabatic temperature change of 0.63 K introduce high entropy perovskite oxides (HEPO) into the field of electric heating for the first time. Liu et al. [38] observed good thermoelectric properties and adiabatic temperature variation in TiO_3 ceramics in a hexagonal system $(\text{Bi}_{1/6}\text{La}_{1/6}\text{Na}_{1/6}\text{K}_{1/6}\text{Sr}_{1/6}\text{Ba}_{1/6}) \Delta T_{\max}$ reaches 0.14 K. In addition, Wang et al. [39] successfully prepared relaxation ferroelectric ceramics of $(\text{Ca}_{0.25}\text{Sr}_{0.25}\text{Ba}_{0.25}\text{La}_{0.25})\text{TiO}_3$ using flash firing technology. The material has a slender hysteresis loop and a discharge energy storage density of 0.684 J/cm³. Although research on the structure and properties of high-entropy perovskite oxides is still in its early stages, they have shown broad application prospects in the field of dielectric ceramics.

6 Conclusion and Outlook

Compared to traditional ceramic materials, high entropy ceramic materials exhibit significant advantages in corrosion resistance, oxidation resistance, thermal stability, and high hardness, making them widely applicable in fields such as national defense, aerospace, and new energy. However, the preparation and theoretical research of high-entropy ceramics still face some challenges:

(1) Synthesis difficulty: The synthesis of high entropy ceramics usually requires complex preparation conditions, such as high temperature, high pressure, or specific gas environments, which limit their wide range of applications.

(2) Cost issue: The production of high-entropy ceramics often relies on multiple rare or expensive elements, which may result in production costs much higher than those of traditional ceramics.

(3) Performance variability: Although some ceramics with high entropy exhibit excellent performance, not all combinations can achieve the expected results, and the consistency and predictability of performance still need to be improved.

(4) Insufficient theoretical research: The theoretical foundation for the stability and performance of

high-entropy ceramics is not yet mature, and more theoretical and experimental research is needed to fully understand their behavior and properties.

In summary, although high-entropy ceramics have shown many promising application areas as an emerging material category, they still face significant challenges. Future research work should focus on improving preparation techniques, reducing production costs, and deepening the understanding of the essential properties of these materials.

References

- [1] Yeh J W, Chen S K, Lin S J, et al. Nanostructured high-entropy alloys with multiple principal elements: novel alloy design concepts and outcomes[J]. *Advanced engineering materials*, 2004,6(5):299-303.
- [2] Rost C M, Sacht E, Borman T, et al. Entropy-stabilized oxides[J]. *Nature communications*, 2015,6(1):8485.
- [3] Djenadic R, Sarkar A, Clemens O, et al. Multicomponent equiatomic rare earth oxides[J]. *Materials Research Letters*, 2017,5(2):102.
- [4] Jiang S, Hu T, Gild J, et al. A new class of high-entropy perovskite oxides[J]. *Scripta Materialia*, 2018,142:116-120.
- [5] Dabrowa J, Stygar M, Mikula A, et al. Synthesis and microstructure of the $(\text{Co,Cr,Fe,Mn,Ni})_3\text{O}_4$ high entropy oxide characterized by spinel structure[J]. *Materials Letters*, 2018,216:32-36.
- [6] Gild J, Zhang Y, Harrington T, et al. High-Entropy Metal Diborides: A New Class of High-Entropy Materials and a New Type of Ultrahigh Temperature Ceramics[J]. *Scientific Reports*, 2016,6(1):37946.
- [7] Elinor C, Csanádi Tamás, Salvatore G, et al. Processing and Properties of High-Entropy Ultra-High Temperature Carbides[J]. *Scientific Reports*, 2018,8(1):8609.
- [8] Qin Y, Liu J X, Li F, et al. A high entropy silicide by reactive spark plasma sintering[J]. *Journal of Advanced Ceramics*, 2019,8(1):148-152.
- [9] Akrami S, Edalati P, Fuji M, et al. High-entropy ceramics: Review of principles, production and applications[J]. *Materials Science and Engineering: R: Reports*, 2021,146:100644.
- [10] Yang Y, HE Q. Lattice distortion in high-entropy alloys[J]. *Acta Metall Sin*, 2020,57(4):385-392.
- [11] Vaidya M, Pradeep K G, Murty B S, et al. Bulk tracer diffusion in CoCrFeNi and CoCrFeMnNi high entropy alloys[J]. *Acta Materialia*, 2018,146:211-224.
- [12] Huang P-K, Yeh J-W. Effects of substrate bias on structure and mechanical properties of $(\text{AlCrNbSiTiV})\text{N}$ coatings[J]. *Journal of Physics D-Applied Physics*, 2009,42(11):115401-115407(7).
- [13] Elinor C, Csanádi T, Salvatore G, et al. Processing and Properties of High-Entropy Ultra-High Temperature Carbides[J]. *Scientific Reports*, 2018,8(1):8609.
- [14] Wang H X, Cao Y J, Liu W, et al. Oxidation behavior of $(\text{Hf}_{0.2}\text{Ta}_{0.2}\text{Zr}_{0.2}\text{Ti}_{0.2}\text{Nb}_{0.2})\text{C-xSiC}$ ceramics at high temperature[J]. *Ceramics International*,

- 2020,46(8):11160-11168.
- [15] Biesuz M, Spiridigliozi L, Dell'Agli G, et al. Synthesis and sintering of (Mg, Co, Ni, Cu, Zn)O entropy-stabilized oxides obtained by wet chemical methods[J]. *Journal of Materials Science*, 2018,53(11):8074-8085.
- [16] Bao S, Chen Y, Hu F Y, et al. Investigation on Microstructure, Wave Absorbing Properties and High Temperature Stability for $(\text{Mg}_{0.2}\text{Ni}_{0.2}\text{Co}_{0.2}\text{Cu}_{0.2}\text{Zn}_{0.2})\text{O}$ High-entropy Ceramics[J]. *Journal of Advanced Ceramics*, 2021:1-16.
- [17] Zhang X S, Xue L Y, Yang F, et al. $(\text{La}_{0.2}\text{Y}_{0.2}\text{Nd}_{0.2}\text{Gd}_{0.2}\text{Sr}_{0.2})\text{CrO}_3$: A novel conductive porous high-entropy ceramic synthesized by the sol-gel method[J]. *Journal of Alloys and Compounds*, 2021,863:158763.
- [18] Wang S, Huo W, Fang F, et al. High entropy alloy/C nanoparticles derived from polymetallic MOF as promising electrocatalysts for alkaline oxygen evolution reaction[J]. *Chemical Engineering Journal*, 2022,429:132410.
- [19] Chu Y, Nin S, Llu D, et al. A (Ta, Nb, Ti, V)C high-entropy carbide nanopowder and its preparation method: CN110407213A[P]. 2019.
- [20] Wang L, Wang Y, Sun X G, et al. Finite element simulation of residual stress of double-ceramic-layer $\text{La}_2\text{Zr}_2\text{O}_7/8\text{YSZ}$ thermal barrier coatings using birth and death element technique[J]. *Computational Materials Science*, 2012,53(1):117-127.
- [21] Lin Z A, Fei L A, Jxl A, et al. High-entropy $\text{A}_2\text{B}_2\text{O}_7$ -type oxide ceramics: A potential immobilising matrix for high-level radioactive waste - ScienceDirect[J]. *Journal of Hazardous Materials*, 2021,(415):125596.
- [22] Riley C, Riva A, Park J, et al. A High Entropy Oxide Designed to Catalyze CO Oxidation Without Precious Metals[J]. *ACS applied materials & interfaces*, 2021, 13(7):8120-8128.
- [23] Hanif M B, Rauf S, ul Abadeen Z, et al. Proton-conducting solid oxide electrolysis cells: Relationship of composition-structure-property their challenges, and prospects[J]. *Matter*, 2023,6(6):1782-1830.
- [24] Jin T, Sang X, Unocic R R, et al. Mechanochemical-Assisted Synthesis of High-Entropy Metal Nitride via a Soft Urea Strategy[J]. *Advanced materials (Deerfield Beach, Fla.)*, 2018,30(23):1707512.
- [25] Gao W, Wang Z, Huang J, et al. Extraordinary thermoelectric performance realized in hierarchically structured AgSbSe_2 with ultralow thermal conductivity[J]. *ACS applied materials & interfaces*, 2018,10(22):18685-18692.
- [26] Zhang P, Lou Z, Qin M, et al. High-entropy $(\text{Ca}_{0.2}\text{Sr}_{0.2}\text{Ba}_{0.2}\text{La}_{0.2}\text{Pb}_{0.2})\text{TiO}_3$ perovskite ceramics with A-site short-range disorder for thermoelectric applications[J]. *Journal of Materials Science & Technology*, 2022,97(02):182-189.
- [27] Riley C, Riva A, Park J, et al. A High Entropy Oxide Designed to Catalyze CO Oxidation Without Precious Metals[J]. *ACS applied materials & interfaces*, 2021,13(7):8120-8128.
- [28] S Roychowdhury. Stabilizing n-Type Cubic GeSe by Entropy-Driven Alloying of AgBiSe_2 :Ultralow Thermal Conductivity and Promising Thermoelectric Performance[J]. *Science Letter*, 2018,130(46):15387-15391.
- [29] Zhou S, Pu Y, Zhang Q, et al. Microstructure and dielectric properties of high entropy $\text{Ba}(\text{Zr}_{0.2}\text{Ti}_{0.2}\text{Sn}_{0.2}\text{Hf}_{0.2}\text{Me}_{0.2})\text{O}_3$ perovskite oxides[J]. *Ceramics International*, 2020,46(6):7430-7437.
- [30] Ma M, Yang X, Meng H, et al. Nanocrystalline high-entropy hexaboride ceramics enable remarkable performance as thermionic emission cathodes[J]. *Fundamental Research*, 2023,3(6):979-987.
- [31] Jiang S, Hu T, Gild J, et al. A new class of high-entropy perovskite oxides[J]. *Scripta Materialia*, 2017,142:116-120.
- [32] Chellali M R, Sarkar A, Nandam S H, et al. On the homogeneity of high entropy oxides: An investigation at the atomic scale[J]. *Scripta Materialia*, 2019,166:58-63.
- [33] Sharma Y, Musico B L, Xiang G, et al. Single-crystal high entropy perovskite oxide epitaxial films[J]. *Physical Review Materials*, 2018,2(6):060404.
- [34] Sarkar A, Djenadic R, Wang D, et al. Rare earth and transition metal based entropy stabilised perovskite type oxides[J]. *Journal of the European Ceramic Society*, 2018,38(5):2318-2327.
- [35] Zhong Y, Sabarou H, Yan X, et al. Exploration of high entropy ceramics (HECs) with computational thermodynamics-A case study with $\text{LaMnO}_3\pm\delta$ [J]. *Materials & Design*, 2019,182:108060.
- [36] Xiong W, Zhang H, Cao S, et al. Low-loss high entropy relaxor-like ferroelectrics with A-site disorder[J]. *Journal of the European Ceramic Society*, 2020,41(4):2979-2985.
- [37] Pu Y, Zhang Q, Li R, et al. Dielectric properties and electrocaloric effect of high-entropy $(\text{Na}_{0.2}\text{Bi}_{0.2}\text{Ba}_{0.2}\text{Sr}_{0.2}\text{Ca}_{0.2})\text{TiO}_3$ ceramic[J]. *Applied Physics Letters*, 2019,115(22):223901.
- [38] Liu W, Li F, Chen G H, et al. Comparative study of phase structure, dielectric properties and electrocaloric effect in novel high-entropy ceramics[J]. *Journal of Materials Science*, 2021,56(33):18417-18429.
- [39] Wang K, Ma B, Li T, et al. Fabrication of high-entropy perovskite oxide by reactive flash sintering[J]. *Ceramics International*, 2020,46(11):18358-18361.

Research Progress of Non-oxide and High Entropy Ceramic Coatings

Junshuai CHEN¹, Yulong WANG¹, Zeyu WANG¹, Xue SHEN¹, Tengyu DU¹, Yubo GONG², Zhigang YANG^{1*}, Gang YU¹

1. Hebei Provincial Engineering Research Center of Metamaterial and Micro-device, School of Materials Science and Engineering, Shijiazhuang Tiedao University, Shijiazhuang, Hebei, 050043 China
2. CARS Engineering Consulting Corporation Limited, Beijing, 100089, China

*Corresponding author: Zhigang YANG, E-mail: yangzhigang@stdu.edu.cn

Abstract

Ceramic coatings play a key role in extending the service life of materials in aerospace and energy fields by protecting materials from high temperature, oxidation, corrosion and thermal stress. Non-oxide and high entropy ceramics are new emerging coating materials which have been researched and developed in recent years. Compared with traditional oxide ceramics, non-oxide ceramics have better high temperature stability, oxidation resistance and erosion resistance. These characteristics make non-oxide ceramics perform well in extreme environments. It is particularly noteworthy that the non-oxide high entropy ceramic is a uniform solid solution composed of at least four or five atoms. Their unique structure and outstanding properties show great potential application in the field of coating. In this paper, the researches about regulating microstructure, preparation technology and properties of nitride and its high entropy system, carbide and its high entropy system and boride and its high entropy system in coating field are summarized, and their future development and prospects are prospected.

Keywords: Nitride; Carbide; Boride; High entropy ceramic coating

1 Introduction

Ceramic coatings as the important technology for surface modification and functional enhancement play a significant role in the field of materials science and engineering. Traditional oxide ceramic coatings such as alumina, titania and so on have achieved widespread applications and remarkable achievements in providing surface protection and enhancing performance. However, with the increasing demand for higher performance and the emergence of new challenges, the researches on novel ceramic coatings are still a hot topic in the current coating field.^[1-7]

As an emerging research direction, non-oxide ceramic coatings and their high-entropy ceramic coatings have attracted widespread attention. Non-oxide ceramic coatings, including carbides, nitrides, and borides, possess excellent high-temperature stability, mechanical properties, and corrosion resistance,^[3-5] making them suitable for applications in various extreme environmental conditions. Additionally, high-entropy ceramic coatings, newly emerging materials, are composed of multiple components and offer more design flexibility and modification capabilities, demonstrating tremendous potential in

material surface modification and performance enhancement.^[2, 8-9]

This review aims to discuss the research progress of non-oxide and their high-entropy ceramic coatings, focusing on the preparation, microstructural characteristics, and performance of nitride and their high-entropy ceramic systems, carbide and their high-entropy ceramic systems, as well as boride and their high-entropy ceramic system coatings. Additionally, an outlook on their future development and prospects is proposed.

2 Nitride Coating Systems

2.1 Binary nitride systems

Binary nitrides possess numerous excellent properties, such as high melting points, structural stability, high mechanical hardness, corrosion resistance, wear resistance, and oxidation resistance. These characteristics make them widely used in various fields,^[10-14] such as cutting tools and hard coatings. Tielidy et al.^[15] deposited titanium nitride on band saw blades using cold plasma technology. Through tribological testing, they found that titanium nitride exhibited low friction coefficients and wear

Copyright © 2024 by author(s). This work is licensed under a Creative Commons Attribution-Noncommercial-No Derivative Works 4.0 License.

Received on May 6, 2024; Accepted on May 29, 2024

values, thereby enhancing the service life of wood cutting tools. Ganeshkumar et al.^[16] deposited silicon nitride coatings on SS304 workpieces, and discovered that knives and blades coated with silicon nitride were more wear-resistant and mechanically superior to those without the coating.

Furthermore, specific preparation processes can significantly influence the coating's properties. Takesue et al.^[17] prepared coatings with high hardness using the atmosphere-controlled induction heating fine particle projection (AIH-FPP) method, improving the wear resistance of low-alloy steel. Additionally, immersion tests in sodium chloride solutions demonstrated their excellent corrosion resistance.

Moreover, some binary nitrides exhibit excellent biocompatibility, making them suitable for applications in medical implants and other fields. Liao et al.^[18] successfully deposited TaN coatings with different nitrogen concentrations on glass slides and medical metal surfaces using magnetron sputtering technology. This coating significantly improved key properties such as adhesion strength, wear resistance, hardness, and biocompatibility. Kim and his team^[19] successfully deposited titanium nitride coatings on vascular stents using reactive magnetron sputtering, significantly enhancing their biocompatibility.

Apart from using binary nitrides directly as coating materials, they can also be used to modify other coating materials through doping or addition to enhance their properties, such as improving crack resistance and corrosion resistance. Qian et al.^[20] successfully synthesized a novel enamel coating by adjusting the content of silicon nitride. The addition of silicon nitride significantly improved the coating's crack resistance while reducing the overall corrosion rate of the materials.

2.2 Multi-element nitride systems

By adding new elements to binary nitride coatings, it is possible to significantly regulate material properties, including crystal orientation, friction performance, and oxidation resistance. The multi-element nitride ceramics provide broad possibilities and development space for the application of coating technology in areas such as friction pairs and high-temperature environments^[21].

Doping new elements into some binary nitrides can alter the crystal orientation of the materials, providing an orientation advantage for the formation of twin crystals and thereby adjusting the mechanical properties of the materials. Yang et al.^[22] deposited $\text{TiB}_{0.11}\text{N}_{1.16}$ coatings on the surface of high-density TBs using direct current magnetron sputtering technology. The doping of boron promoted the orientation transition of the coatings. Compared to the function of TiN as the coating, this approach resulted in higher hardness and toughness.

The doping of some metal elements can change the oxidation resistance of materials. For example,

appropriate doping of Al elements can improve the oxidation resistance of materials, making them suitable for applications in metal processing and the aviation industry. Makgae et al.^[23] doped Al elements into TiN coatings to prepare $\text{Ti}_{1-x}\text{Al}_x\text{N}$ coatings. When $X=0.44$, the coverage on the coating was the highest, making the $\text{Ti}_{0.56}\text{Al}_{0.44}\text{N}$ component become the most oxidation-resistant coating. Zhang et al.^[24] added Ni to CrN coatings, and the alloying of Ni significantly reduced the surface roughness of the coatings, improved their toughness, and increased the critical fracture stress of CrN coatings. This method reduced the fatigue crack length caused by CrN coating fractures in the substrate, making an important contribution to the widespread application of nitride sand-resistant coatings in the compressor area of aero-engines. Zhang et al.^[25] deposited wear-resistant and corrosion-resistant binary TiN and ternary TiZrN coatings using high-power pulsed magnetron sputtering (HiPIMS) technology. It was found that ternary TiZrN exhibited higher surface hardness, elastic modulus and excellent resistance to degradation in acidic solutions.

Moreover, multi-layer coating possesses superior properties compared to single-layer coating. Meanwhile, multi-layer structures have more complex orientations than single-layer structures, and coatings with mixed orientations exhibit better mechanical properties than those with a single orientation. Ma et al.^[26] successfully prepared TiZrN coatings on Ti-6Al-4V alloy surfaces using arc plasma deposition technology, demonstrating that coatings with mixed orientations exhibit better strength and toughness than those with a single orientation. Wang et al.^[10] prepared a 12 μm Cr/CrN/Cr/CrAlN corrosion-resistant multi-layer coating using arc ion plating. Under high-temperature conditions, the multi-layer coating exhibited superior high-temperature impact resistance and erosion resistance compared to single-layer coatings. At 700°C, the coating remained stable and unchanged, meeting the operating requirements of gas turbine compressor blades. Maksakova et al.^[27] deposited multi-layer TiZrN/TiSiN coatings on steel substrates using cathodic arc evaporation. Compared to TiZrN and TiSiN films, the multi-layer films exhibited higher hardness of up to 38.2 ± 1.15 GPa and elastic modulus of up to 430 ± 2.9 GPa, demonstrating higher resistance to plastic deformation. Chema et al.^[28] performed nitriding treatment on four-layer 304L stainless steel multi-layer coatings deposited using the TWAS process using duplex treatment (PIII+PVD-deposited W-Ti-N coatings). They found that the W-Ti-N coatings exhibited excellent performance in terms of hardness, friction coefficient, and wear rate, indicating the potential for applying this process to austenitic stainless steel.

In summary, in recent years, researches about multi-element nitride coating materials have developed rapidly. By regulating their structure, mechanical

properties, corrosion resistance, and other characteristics, new possibilities for enhancing material performance and expanding their applications are provided.

2.3 High-entropy nitride systems

High-entropy ceramics are new multi-component ceramic materials, and their design concept is first derived from high-entropy alloys. The fatigue resistance, corrosion resistance, and mechanical properties can be enhanced through the increase of entropy in high-entropy ceramics. Compared with traditional ceramics, high-entropy ceramics achieve the high-entropy effect by mixing multiple components in equal atomic ratios to form a uniform lattice structure. Among the various high-entropy ceramic coatings, high-entropy nitride coatings exhibit higher hardness, wear resistance, chemical stability, adhesion, excellent thermal conductivity, and multifunctionality. These advantages make high-entropy nitride coatings promising for a wide range of applications in coating technology, providing enhanced and reliable protection and performance enhancement^[29-37].

In 2019, Hahn et al.^[38] used DC magnetron sputtering to prepare a single-phase (Al,Ta,Ti,V,Zr)N high-entropy nitride coating with nearly equimolar metal components. The coating exhibited a hardness of 30 GPa and a fracture toughness of 2.4 MPa m^{1/2}. In 2020, Moskovskikh et al.^[39] utilized mechanically activated nanostructured metal precursors to obtain high-entropy nitride phases through exothermic combustion in nitrogen and consolidated them through spark plasma sintering. The high-entropy nitride (Hf_{0.2}Nb_{0.2}Ta_{0.2}Ti_{0.2}Zr_{0.2})N coating had a hardness of up to 33 GPa and a fracture toughness of up to 5.2 MPa m^{1/2}, which was suitable for applications in superhard coating fields.

The increasing researches have significantly improved the properties of materials through optimized preparation processes. Compared with magnetron sputtering^[40-43], MAIP (Magnetron Arc Ion Plating) offers several advantages, including excellent adhesion to the substrate, outstanding diffusion deposition performance, and rapid deposition speed. Xu et al.^[44] used a multi-arc ion plating (MAIP) system to deposit a high-entropy ceramic (TiCrZrVAl)N coating on the surface of an alloy. The coating had a maximum hardness of 31.08±1.81 GPa and an elastic modulus of 387.66±12.49 GPa, exhibiting excellent wear resistance with a minimum wear rate of 7.4×10⁻¹⁶ m³/(N m). The design strategy of high-entropy nitrides provides an optimized solution for nuclear fuel cladding materials. Wang et al.^[45] used magnetron sputtering to prepare TiNbZrTaN/CrFeCoNiN_x nitride multilayer films, which exhibited high crystallinity, structural stability, and diffusion resistance under high temperature and irradiation conditions. These findings can be explained by difference in atomic size, Gibbs free

energy in mixed systems, and solute-induced chemical inhomogeneity. Moreover, the performance of materials can be improved through the crystal orientation. Lu et al.^[46] prepared (CrAlTiNbV)N_x coatings using magnetron sputtering, which was shown in Figure 1(a) and (b). As the substrate bias increased, the coating transformed from a loosely packed columnar crystal structure with a preferred (200) orientation to a dense nanocrystalline structure. In Figure 1(c) and (d), at the substrate biases of -96 V and -126 V, the coating exhibited the lowest average friction coefficient (around 0.06) and wear rate 8.7×10⁻⁹ mm³ / (N m).

Recently, machine learning methods have been introduced into the study of high-entropy nitride coatings. Machine learning can be used to predict the properties of high-entropy materials. By collecting and organizing a large amount of experimental data or simulation results from known high-entropy materials, a machine learning model can be constructed. This model can analyze the composition, structural parameters, and correlations of materials, and infer performance characteristics associated with these features, such as the hardness, modulus, and wear resistance of high-entropy nitride coatings. Zhou et al.^[47] proposed a data augmentation generative adversarial network (DAGAN)-driven machine learning (ML) design strategy to predict the hardness, modulus, and wear resistance of novel HEN compounds.

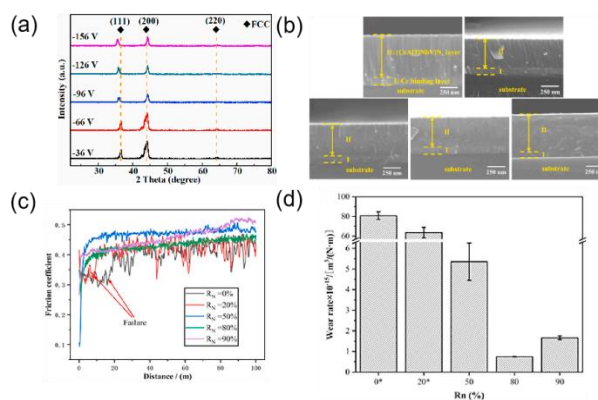


Figure 1 (a) XRD patterns of (CrAlTiNbV)N_x coatings versus substrate bias, (b) SEM cross-section images of (CrAlTiNbV)N_x coatings fabricated at various substrate biases, (c) friction curve of (TiCrZrVAl)N films, (d) wear rate of (TiCrZrVAl)N films^[46]

3 Carbide Coating System

3.1 Binary carbide system

Binary carbides possess numerous excellent properties such as wear resistance, high hardness, and corrosion resistance, among which wear resistance stands out as a particularly noteworthy feature. Especially for wear resistance (the abrasion resistance of carbide coatings),

binary carbides can be applied in various fields, such as enhancing the service life of cold and hot forging, extrusion, and powder metallurgy molds under abrasive forces.

Micallef et al. [48] employed chemical vapor deposition to deposit tungsten carbide on demanding components. Through corrosion and tribological tests, they discovered that tungsten carbide exhibited a uniform coating structure, which differed from traditional cemented coatings. The low friction coefficient and corrosion rate of tungsten carbide broaden the application prospects. One of the main potential research directions in the future is binder-free tungsten carbide coatings with sub-micron surface smoothness. Zhao et al. [49] thermally pressed niobium with cast iron at high temperatures and used interstitial carburization to precipitate NbC and Nb₂C on the substrate surface, forming a ceramic coating. Observations showed that scratches were not evident on the substrate with the niobium coating. Although the loading of the substrate led to plastic deformation, the coating only peeled off when the surface bearing capacity reached 100 N, indicating strong adhesion between the coating and the substrate (> 100 N). Hardness tests revealed a significant improvement in hardness after applying niobium to the substrate. Apart from chemical deposition and surface carburization, Khan et al. [50] employed an in-situ coating method to coat titanium carbide on graphene nanoplates (GNPs). This approach reduced wetting between GNPs and aluminum while enhanced dispersibility. Liu et al. [51] used plasma electrolytic oxidation (PEO) to prepare a titanium carbide coating on aluminum alloy surfaces. TiC particles enhanced the corrosion resistance of PEO coatings of aluminum alloy. Therefore, utilizing PEO technology to coat TiC on aluminum alloy tubing to improve the corrosion resistance of aluminum alloy oil well pipes is both novel and promising.

In addition to using binary carbides directly as coating materials, they can also be doped into other material coating to improve the performance. Chen et al. [52] studied the effects of adding tungsten carbide to graphite coatings on wear resistance and lubrication. They found that when adding 30% tungsten carbide, the graphite coating achieved a good balance in various performance using flame spraying technology.

3.2 Multi-component carbide system

In complex environments with stringent requirements, the performance of materials often needs to be further enhanced based on specific needs and practical situations. The multiple elements in carbide can further improve the properties, enabling their application in various fields such as industry, manufacturing, biology and so on. Therefore, the formation of multi-component carbide coatings on the surface of parts is a practical approach to meet high demands [53]. Li et al. [54] employed the powder immersion reaction method to coat graphite

with chromium carbide and niobium carbide. Through studying the microstructure and mechanical properties of the coating, an optimal elemental ratio of 50% chromium carbide and 50% niobium carbide was obtained. The addition of chromium and niobium elements improved the mechanical properties of graphite. Furthermore, within a certain temperature range, the thermal expansion coefficient of the coating is basically consistent with that of the graphite substrate, facilitating good adhesion and preventing peeling.

Some carbides coatings also exhibit the biocompatibility, such as titanium carbide niobium with high corrosion resistance and wear resistance. Pana et al. [55] used cathodic arc evaporation to prepare the coatings for implants on stainless steel substrates. It was found that the titanium carbide niobium coating exhibited the smallest grain size, lowest roughness, low wear rate, highest hardness and adhesion, relatively low porosity, and good corrosion resistance. The niobium-containing titanium carbide coatings as a promising bio-coating has broad application prospects in biological field. Tungsten carbide, a compound with high hardness and thermal conductivity, is widely used as a coating for cutting tools. Based on the high-speed oxygen-fuel spraying process, Govande et al. [56] introduced cobalt into this coating and further conducted low-temperature treatment. The results showed that low-temperature treatment improved the wear resistance of the coating. The densification of the cobalt matrix further enhanced the wear resistance of the coating. Additionally, the coating exhibited better corrosion resistance after low-temperature treatment.

In summary, researches on multi-component carbide coating materials have developed rapidly in recent years. Coating materials with multi-component carbides can enhance their mechanical properties, wear resistance, and corrosion resistance. New exploration of multi-component carbides including component, processing technology, microstructure and properties is still urgent, aiming to further promote the real applications.

3.3 High-entropy carbide systems

High-entropy carbide ceramic coatings possess extremely high hardness, wear resistance, and excellent ablation resistance [34-37, 57]. These characteristics make them applied in aerospace, chemical industries, and other fields [29-30, 32, 58]. Wang et al. [59] prepared (Hf-Ta-Zr-Nb)C high-entropy carbide with excellent mechanical erosion resistance and oxidation-controlled ablation mechanisms at 2100°C using a plasma flame gun, becoming an ideal candidate for UHTC. Chen et al. [60] prepared porous high-entropy (Hf_{0.2}Zr_{0.2}Nb_{0.2}Ta_{0.2}Ti_{0.2})C ceramics using an in-situ reaction/partial sintering method. Figure 2(a) and (b) showed SEM images of porous (Zr_{0.2}Hf_{0.2}Ti_{0.2}Nb_{0.2}Ta_{0.2})C before and after annealing at

1850°C. The porous structure and grain size of the samples did not change significantly after annealing, and no significant grain growth was observed due to the retarded diffusion effect, indicating good high-temperature stability of the porous high-entropy carbide ceramics. Figure 2(c) shows the XRD patterns of $(\text{Zr}_{0.2}\text{Hf}_{0.2}\text{Ti}_{0.2}\text{Nb}_{0.2}\text{Ta}_{0.2})\text{C}$ sample before and after annealing at 1850°C. The phase composition of the sample still remained to be high-entropy $(\text{Zr}_{0.2}\text{Hf}_{0.2}\text{Ti}_{0.2}\text{Nb}_{0.2}\text{Ta}_{0.2})\text{C}$ phase without phase decomposition or phase transformation, demonstrating excellent phase stability. Figure 2 (d) shows a plot of the linear shrinkage rate (dL/L_0) as a function of temperature. It can be seen that no significant size changes during heating, indicating excellent dimensional stability of the porous high-entropy $(\text{Zr}_{0.2}\text{Hf}_{0.2}\text{Ti}_{0.2}\text{Nb}_{0.2}\text{Ta}_{0.2})\text{C}$ ceramics.

High-entropy carbide ceramics exhibit excellent high-temperature radiation resistance and can be used in future advanced nuclear systems. Zhu et al. [61] prepared high-entropy carbide ceramics $(\text{WTiVNbTa})\text{C}_5$ using spark plasma sintering, and they were irradiated with 1.0 MeV c-ions at room temperature and 650°C. No amorphization or cavity formation was observed in all samples after irradiation, demonstrating that they had high radiation resistance at high temperatures. Tunes et al. [62] synthesized a novel carbide CrNbTaTiW using magnetron sputtering. The synthesized material with the carbon content of about 50 at.% exhibited the nanocrystalline with single-phase crystal structure. In-situ transmission electron microscopy was used to investigate the irradiation response of the novel high-entropy carbide (HEC) at 573 K, which exhibited better radiation tolerance than high-entropy alloys.

Moreover, the high-entropy carbide ceramic matrix composites prepared through the combination with other materials have excellent performance, realizing the widely applications in new fields. For instance, Zhang et al. [63] employed discharge plasma sintering technology to fabricate $(\text{VNbTaMoW})\text{C}_5\text{-SiC}$ high-entropy ceramics under conditions of 1900 °C and 40 MPa. With the increase in SiC content, the hardness of $(\text{VNbTaMoW})\text{C}_5\text{-SiC}$ multiphase ceramics increased, while the fracture toughness first increased and then decreased. $(\text{VNbTaMoW})\text{C}_5\text{-20 wt.% SiC}$ exhibited the best mechanical properties, with vickers hardness and fracture toughness of 18.2 GPa and 5.7 $\text{MPa m}^{1/2}$, respectively. Cai et al. [64] prepared $\text{Cf}/(\text{Ti}_{0.2}\text{Zr}_{0.2}\text{Hf}_{0.2}\text{Nb}_{0.2}\text{Ta}_{0.2})\text{C-SiC}$ high-entropy ceramic matrix composites using the precursor infiltration pyrolysis (PIP) method, which exhibited excellent ablation resistance with a linear recession rate of $\sim 2.89 \mu\text{m/s}$ and a mass recession rate of $\sim 2.60 \text{ mg/s}$. This was primarily attributed to the formation of a dense and stable oxide layer on the surface of the sample. Luo et al. [65] fabricated high-entropy $(\text{Ti,Zr,Nb,Ta,Mo})\text{C-Co}$

composites using liquid-phase sintering. When the initial sintering aid was 10 vol% Co, the densification temperature could be reduced to 1350 °C due to liquid-phase sintering. Compared to solid-state sintered $(\text{Ti,Zr,Nb,Ta,Mo})\text{C}$ ceramics prepared under conditions of 2000 °C and 35 MPa, the hardness slightly decreased from $25.06 \pm 0.32 \text{ GPa}$ to $24.11 \pm 0.75 \text{ GPa}$, but the toughness increased from $2.25 \pm 0.22 \text{ MPa m}^{1/2}$ to $4.07 \pm 0.13 \text{ MPa m}^{1/2}$. Significantly reducing the sintering temperature can bring benefits such as energy conservation, improved production efficiency, and reduced material loss. Recently, the combination of simulation calculations and experimental preparation is a commonly used and effective research method for providing a more comprehensive understanding and explanation of material properties, reaction mechanisms, and other related issues. Ye et al. [66] analyzed the formation possibility of novel $(\text{Zr}_{0.25}\text{Nb}_{0.25}\text{Ti}_{0.25}\text{V}_{0.25})\text{C}$ high-entropy ceramics through first-principles calculations and thermodynamic analysis. They successfully prepared this high-entropy ceramic using hot-pressing sintering, which exhibited high hardness, elastic modulus, and fracture toughness.

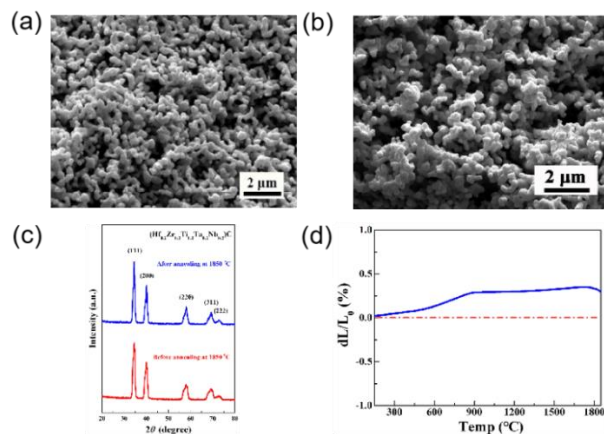


Figure 2 (a-b) SEM micrograph of porous $(\text{Zr}_{0.2}\text{Hf}_{0.2}\text{Ti}_{0.2}\text{Nb}_{0.2}\text{Ta}_{0.2})\text{C}$ sample before and after annealing, (c) XRD patterns of the $(\text{Zr}_{0.2}\text{Hf}_{0.2}\text{Ti}_{0.2}\text{Nb}_{0.2}\text{Ta}_{0.2})\text{C}$ before and after annealing at 1850 °C, (d) The dL/L_0 curve of porous $(\text{Zr}_{0.2}\text{Hf}_{0.2}\text{Ti}_{0.2}\text{Nb}_{0.2}\text{Ta}_{0.2})\text{C}$ [60]

4 Boride Coating Systems

4.1 Binary boride systems

Boride coatings are currently one of the most extensively studied materials in the field of ceramic coatings, including zirconium boride, hafnium boride, and titanium boride. Borides have excellent properties such as corrosion resistance, wear resistance, and excellent oxidation resistance at high temperatures. For instance, boride coatings were coated on surface of metal materials like iron through thermal spraying and

infiltration technology, which could significantly improve the tribological properties while enhancing their microhardness. Lindner et al. [67] employed the powder pack infiltration method to harden high-speed oxygen-fuel sprayed Inconel 625 coatings. Further thermochemical treatment was also adopted to intensify the coatings, resulting in a significant increase in microhardness and wear resistance. Khater et al. [57] investigated the mechanical and tribological properties of titanium boride coatings obtained through thermochemical boriding in a salt bath composed of 70% borax and 30% silicon carbide. They found that boriding at 1000 °C for 8 hours obtained the highest TiB₂ layer thickness, which reached a value of 50 μm. The formation of the TiB₂ layer increased the surface hardness and elastic modulus of the substrate by 9 times and 2.5 times, respectively, offering a new approach to enhancing the performance of matrix materials or parts. Mirhosseini et al. [68] successfully deposited Al₂O₃-TiB₂ coating on surface of steel substrate using in-situ plasma spraying (IPS). The Al₂O₃-TiB₂ coating exhibited excellent mechanical properties with a hardness of 797.6 HV, a wear track width of 1061.3 μm, and a wear rate of $4.2 \times 10^3 \text{ mm}^3 / (\text{N m})$.

Additionally, the properties of boride ceramics can be improved by doping other materials. Zeng et al. [69] prepared metal boride MB_x (M = V, Mo, and Fe) and MnO₂ co-doped NiCr₂O₄ coatings using atmospheric pressure plasma spraying. These coatings exhibited excellent infrared emissivity within the range of 5 ~ 25 μm and also demonstrated good heat resistance. Salyi et al. [70] employed powder pack infiltration boriding to form boride coatings on steel samples. Both the Fe₂B and FeB phases exhibited excellent corrosion resistance.

4.2 Multi-component boride systems

With the continuous advancement of industrial technology, the demand for high-performance materials is becoming increasingly urgent. Multi-component borides, as a class of promising materials, will play a significant role in various fields. Although the performance of multi-component borides has been significantly improved, the optimization of their preparation processes and further enhancement of their comprehensive properties remains to be issues that need to be addressed in current research to promote their wider application and development.

By reasonably controlling the process parameters, high-quality multi-component boride cladding layers can be obtained, exhibiting excellent adhesion, compactness, and metallurgical bonding. Zhang et al. [71] studied the relationship between the input process parameters (laser power, scanning speed, pre-laid thickness) and the output responses (height, width, dilution rate) of Mo₂FeB₂ coatings through sensitivity analysis. The results showed that laser power had a

positive effect on the coating width and dilution rate, while having a negative effect on the coating height. Apart from process regulation, modifying the coating composition can also enhance its performance. Bao et al. [72] prepared the composite coating resistant to high-temperature zinc-aluminum molten liquid corrosion using supersonic flame spraying. Mo-B₄C powders were mixed with WC and Co powders with different proportion to prepare composite powders. An appropriate amount of Mo-B₄C reacted with Co to form ternary borides such as CoMo₂B₂ and CoMoB. These ternary borides could formed a perfect and continuous interface, improving the mechanical properties and corrosion resistance of the coating.

4.3 High-entropy boride systems

Currently, researches on high-entropy boride coatings are relatively limited and still in the developing stage. However, due to their outstanding comprehensive properties such as high hardness, high melting point, and excellent corrosion resistance, high-entropy borides are expected to play a significant role in the field of ceramic coatings [73-77]. Mayrhofer et al. [78] prepared ZrB₂, (Zr,Ti)B₂, and (Zr,V,Ti,Ta,Hf)B₂ coatings using non-reactive magnetron sputtering. Figure 3(a) demonstrated that the prepared boride ceramic coatings exhibit single-phase solid solution. Figure 3(b) showed that the three diboride coatings exhibited very dense morphologies. Compared to ZrB₂ and (Zr,Ti)B₂, the (Zr,Ti,Hf,V,Ta)B₂ coating exhibited the highest hardness (47.2±1.8 GPa). Zhang et al. [79] employed the gas reaction infiltration-assisted slurry spraying (GRSI-SP) method to in situ deposit the high-entropy (Hf_{0.25}Zr_{0.25}Ti_{0.25}Cr_{0.25})B₂ ceramic-modified SiC-Si (HETMB₂-SiC-Si) coating on the surface of carbon/carbon (C/C) composites to enhance their oxidation resistance at 1973 K. Subsequently, dynamic ablation tests were conducted at ultra-high temperatures (up to 2404 K) using an oxy-acetylene torch (OAT) to investigate the ablation behavior and protective mechanism of the composite coating on C/C composites. Different oxidation deposition were formed under different ablation regions, enhancing high-temperature thermal stability. This study provides the guidance for exploring the heat resistance of high-entropy boride ceramic coatings as high-temperature thermal protection systems under severe conditions. Recently, Guo et al. [80] prepared a multi-component boride (Hf_{0.5}Zr_{0.5})B₂-SmB₆-ErB₄-YB₆ (HZRB) coating on the surface of SiC-coated carbon/carbon (C/C) composites using supersonic atmospheric plasma spraying. The excellent ablation resistance was primarily attributed to the formation of a high-density (Hf_{0.2}Zr_{0.2}Sm_{0.2}Er_{0.2}Y_{0.2})O_{2-δ} high-entropy oxide (HEO) layer during the ablation process.

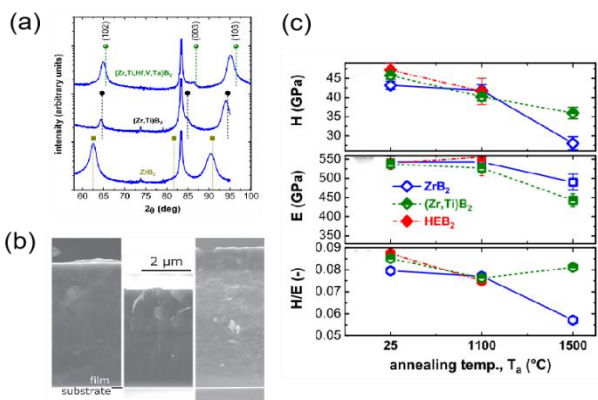


Figure 3 (a) XRD images(b)SEM images; (C)Hardness, indentation modulus and their corresponding ratios of ZrB_2 , $Zr_{0.61}Ti_{0.39}B_2$, and $Zr_{0.23}Ti_{0.20}Hf_{0.19}V_{0.14}Ta_{0.24}B_2$ thin films [78]

5 Conclusion and Outlook

Non-oxide ceramics including carbides and their high-entropy ceramics, nitrides and their high-entropy ceramics, as well as borides and their high-entropy ceramics, possessed high hardness, excellent high-temperature resistance, corrosion resistance, and other properties. These characteristics made them application prospects in the field of ceramic coatings. Composition regulation engineering offered significant opportunities to improve the performance of ceramic coatings and promote their applications. The development from binary systems, multi-component coating systems to high-entropy ceramic coating systems had been accompanied by continuous optimization of their properties. In particular, the recently developed high-entropy ceramic coating system had achieved significant innovation in coating materials. High-entropy coatings exhibited advantages such as higher high-temperature stability, corrosion resistance, hardness, and wear resistance, meeting the needs of more application areas and showing broad prospects and tremendous potential. Currently, the regulations of coating composition, coating structure, and internal crystal orientation within the coating are hot research directions, and breakthrough progresses have been achieved. However, the non-oxide ceramic system was still imperfect, especially the researches on high-entropy non-oxide ceramic systems were relatively scarce. The following directions will be developed [79-80].

(1) In the design of non-oxide ceramic coating systems, the introduction of theoretical calculations such as first principles and machine learning can achieve theoretical guidance for experiments, avoiding the need for conducting a large number of experiments. This is conducive to reducing costs and improving research and development efficiency. It also helps to gain a deeper understanding of the properties of high-entropy ceramics. This will provide important guidance for the research

and development of non-oxide and their high-entropy ceramic coatings.

(2) The optimization, improvement, and innovation of the preparation processes for non-oxides and their high-entropy ceramic coatings are also critical issues that need to be addressed urgently. Through the optimization and innovation of preparation processes, controllable preparation of high-performance non-oxide coatings can be achieved, enhancing the efficiency of coating preparation and reducing preparation costs.

(3) There exist less researches on the high-temperature mechanical properties, radiation resistance, ablation resistance, and other service properties of non-oxides and their high-entropy ceramic coatings, which need to be further researched to realize their applications.

References

- [1] BAZHIN P M, TITOV N V, ZHIDOVICH A O, et al. Features of the carbo-vibroarc surfacing in the development of multicomponent cermet wear-resistant coatings[J]. *Surface and Coatings Technology*, 2022(429):12795.
- [2] BODNYA I S, TIMOSHENKO V P. Numerical modeling of a wing leading-edge thermal regimes for a reusable space vehicle[J]. *RUDN Journal of Engineering Researches*, 2018,19(1):7-21.
- [3] RICHARDSON P J, KEAST V J, CUSKELLY D T, et al. Theoretical and experimental investigation of the W-Al-B and Mo-Al-B systems to approach bulk WAIB synthesis[J]. *Journal of the European Ceramic Society*, 2021,41(3):1859-1868.
- [4] CHENG Y, HU P, DONG S, et al. Dual bionics of structure and preparation: Gradient architected carbon/ceramic composite as light as water but bearing ultra-high temperature max to 2500 C[J]. *Composites Part B: Engineering*, 2023(265):110963.
- [5] LI C, FAN H, NI L, et al. Phase transformation and thermal conductivity of the APS Y_2O_3 doped HfO_2 coating with hybrid structure[J]. *Ceramics International*, 2022,48(14):19633-19643.
- [6] CUI Y J, LI J E, WANG B L, et al. Thermally induced delamination and buckling of a ceramic coating with temperature-dependent material properties from porous substrate at high temperatures[J]. *Acta Mechanica*, 2020,231(6):2143-2154.
- [7] Yang Y Z, Yang J I, Fang D N. Research progress on thermal protection materials and structures of hypersonic vehicles[J]. *Applied Mathematics and Mechanics*, 2008,29(1):51-60.
- [8] Gorr B, Schellert S, Muller F, et al. Current Status of Research on the Oxidation Behavior of Refractory High Entropy Alloys[J]. *Advanced Engineering materials*, 2021,23(5):2001047.
- [9] Yang S Q, Yang H Z, Shi Q, et al. Investigation on failure mechanism and interfacial diffusion behavior of NiCoCrAlYTa coating at high temperature[J]. *Coeosion Science*, 2024,229:111871.

- [10] WANG D, LIN S-S, DUAN D-Y, et al. Thermal shock resistance of Cr/CrN/Cr/CrAlN multilayer anti-erosion coating[J]. *Surface and Coatings Technology*, 2023(470):129776.
- [11] ZAKUTAYEV A, PERKINS C L. Influence of Protection Layers on Thermal Stability of Nitride Thin Films[J]. *physica status solidi (RRL)-Rapid Research Letters*, 2021,15(8):2100178.
- [12] REN J, XU L, LUO J, et al. Hydrothermal oxidation of titanium nitride coating for enhanced corrosion resistance in fluoride-containing acidic solution[J]. *Materials Letters*, 2023(335): 133790.
- [13] BAKKAR S, ZUCHA E, BEAM J, et al. A new approach to protect and extend longevity of the thermal barrier coating by an impermeable layer of silicon nitride[J]. *Journal of the American Ceramic Society*, 2023,106(10):6221-6229.
- [14] SAJI V S. 2D hexagonal boron nitride (h-BN) nanosheets in protective coatings: A literature review[J]. *Heliyon*, 2023,9(9):19362.
- [15] DE LIMA T A D M, DE LIMA G G, DA COSTA L N, et al. Evaluation of titanium nitride coatings in bandsaw blades for wood splitting by cold plasma[J]. *Wood Material Science & Engineering*, 2021,18(1):130-140.
- [16] GANESHKUMAR S, SINGH B K, KUMAR S D, et al. Study of Wear, Stress and Vibration Characteristics of Silicon Carbide Tool Inserts and Nano Multi-Layered Titanium Nitride-Coated Cutting Tool Inserts in Turning of SS304 Steels[J]. *Materials (Basel)*, 2022,15(22):7994-8006.
- [17] TAKESUE S, MORITA T, MISAKA Y, et al. Rapid formation of titanium nitride coating by atmospheric-controlled induction-heating fine particle peening and investigation of its wear and corrosion resistance[J]. *Results in Surfaces and Interfaces*, 2023(11):100121.
- [18] LIAO S, YANG L, SONG Z, et al. Effect of nitrogen content on the mechanical and biological properties of tantalum nitride coatings[J]. *Surface and Coatings Technology*, 2023(464): 129544.
- [19] KIM I I, SUROVTSEVA M A, POVESHCHENKO O V, et al. Biocompatibility of Titanium Oxynitride Coatings Deposited by Reactive Magnetron Sputtering[J]. *Bulletin of Experimental Biology and Medicine*, 2022,173(6):779-782.
- [20] QIAN H, CHEN S, WANG T, et al. Silicon nitride modified enamel coatings enable high thermal shock and corrosion resistances for steel protection[J]. *Surface and Coatings Technology*, 2021(421):127474.
- [21] YAN P, CHEN K, WANG Y, et al. Design and Performance of Property Gradient Ternary Nitride Coating Based on Process Control[J]. *Materials*, 2018,11(5):758-770.
- [22] YANG S, GUO T, YAN X, et al. High-density twin boundaries in transition metal nitride coating with boron doping[J]. *Acta Materialia*, 2023(255):119033.
- [23] MAKGAE O A, LENRICK F, BUSHLYA V, et al. Visualising microstructural dynamics of titanium aluminium nitride coatings under variable-temperature oxidation[J]. *Applied Surface Science*, 2023(618):156625.
- [24] ZHANG Z, YANG Z, HE G. Alleviating the adverse influence of nitride coating on the fatigue performance of Ti6Al4V by Ni alloying[J]. *Journal of Materials Research and Technology*, 2023(26):517-529.
- [25] ZHANG Y L, CHEN F, ZHANG Y, et al. Corrosion and tribocorrosion behaviors of ternary TiZrN coating on 304 stainless steel prepared by HiPIMS[J]. *Materials Today Communications*, 2022(31):103258.
- [26] MA A, LIU D, ZHANG X, et al. Solid particle erosion behavior and failure mechanism of TiZrN coatings for Ti-6Al-4V alloy[J]. *Surface and Coatings Technology*, 2021(426):127701.
- [27] MAKSAKOVA O V, ZHANYSSOV S, PLOTNIKOV S V, et al. Microstructure and tribomechanical properties of multilayer TiZrN/TiSiN composite coatings with nanoscale architecture by cathodic-arc evaporation[J]. *Journal of Materials Science*, 2020,56(8):5067-5081.
- [28] CHEMAA K, HASSANI S, KEZRANE M, et al. Tribological Investigation of W-Ti-N Thin Film on Plasma Nitrided Stainless-Steel Multilayer Coating[J]. *Jom*, 2023,75(8):3111-3120.
- [29] STASIAK T, SOUČEK P, BURŠÍKOVÁ V, et al. Synthesis and characterization of the ceramic refractory metal high entropy nitride thin films from Cr-Hf-Mo-Ta-W system[J]. *Surface and Coatings Technology*, 2022(449):128987.
- [30] HSU S Y, LAI Y T, CHANG S Y, et al. Combinatorial synthesis of reactively co-sputtered high entropy nitride (HfNbTiVZr)N coatings: Microstructure and mechanical properties[J]. *Surface and Coatings Technology*, 2022(442):128564.
- [31] DIPPO O F, MESGARZADEH N, HARRINGTON T J, et al. Bulk high-entropy nitrides and carbonitrides[J]. *Scientific Reports*, 2020,10(1):21288.
- [32] LI F, CUI W, SHAO Y, et al. Preparing high-entropy ceramic films from high-entropy alloy substrate[J]. *Materials Chemistry and Physics*, 2022(287):126365.
- [33] KRETSCHMER A, BOHRN F, HUTTER H, et al. Analysis of (Al,Cr,Nb,Ta,Ti)-nitride and -oxynitride diffusion barriers in Cu-Si interconnects by 3D-Secondary Ion Mass Spectrometry[J]. *Materials Characterization*, 2023(197):112676.
- [34] NI D, CHENG Y, ZHANG J, et al. Advances in ultra-high temperature ceramics, composites, and coatings[J]. *Journal of Advanced Ceramics*, 2021,11(1):1-56.
- [35] WU S, XU X, YANG S, et al. Data-driven optimization of hardness and toughness of high-entropy nitride coatings[J]. *Ceramics International*, 2023,49(13):21561-21569.
- [36] SI Y, WANG G, WEN M, et al. Corrosion and friction resistance of TiVCrZrWN_x high entropy ceramics coatings prepared by magnetron sputtering[J]. *Ceramics International*, 2022,48(7):9342-9352.
- [37] REN B, ZHAO R F, ZHANG G P, et al. Microstructure and properties of the AlCrMoZrTi/(AlCrMoZrTi)N multilayer high-entropy nitride ceramics films deposited by reactive RF sputtering[J]. *Ceramics International*, 2022,48(12):16901-16911.
- [38] HAHN R, KIRNBAUER A, BARTOSIK M, et al. Toughness of Si alloyed high-entropy nitride coatings[J]. *Materials Letters*, 2019(251):238-240.
- [39] MOSKOVSKIKH D, VOROTILO S, BUINEVICH V, et al.

- Extremely hard and tough high entropy nitride ceramics[J]. *Scientific Reports*, 2020,10(1):19874.
- [40] CHANG C H, YANG C B, SUNG C C, et al. Structure and tribological behavior of (AlCrNbSiTiV)N film deposited using direct current magnetron sputtering and high power impulse magnetron sputtering[J]. *Thin Solid Films*, 2018(668):63-68.
- [41] CHEN T K, WONG M S, SHUN T T, et al. Nanostructured nitride films of multi-element high-entropy alloys by reactive DC sputtering[J]. *Surface and Coatings Technology*, 2005,200(5-6):1361-1365.
- [42] BRAIC V, VLADESCU A, BALACEANU M, et al. Nanostructured multi-element (TiZrNbHfTa)N and (TiZrNbHfTa)C hard coatings[J]. *Surface and Coatings Technology*, 2012(211):117-121.
- [43] FENG X, ZHANG K, ZHENG Y, et al. Chemical state, structure and mechanical properties of multi-element (CrTaNbMoV)_{N_x} films by reactive magnetron sputtering[J]. *Materials Chemistry and Physics*, 2020(239):121991.
- [44] XU W, LIAO M, LIU X, et al. Microstructures and properties of (TiCrZrVAl)N high entropy ceramics films by multi-arc ion plating[J]. *Ceramics International*, 2021,47(17):24752-24759.
- [45] WANG J, SHU R, CHAI J, et al. Xe-ion-irradiation-induced structural transitions and elemental diffusion in high-entropy alloy and nitride thin-film multilayers[J]. *Materials & Design*, 2022(219):110749.
- [46] LU X, ZHANG C, ZHANG X, et al. Dependence of mechanical and tribological performance on the microstructure of (CrAlTiNbV)_{N_x} high-entropy nitride coatings in aviation lubricant[J]. *Ceramics International*, 2021,47(19):27342-27350.
- [47] ZHOU Q, XU F, GAO C, et al. Design of high-performance high-entropy nitride ceramics via machine learning-driven strategy[J]. *Ceramics International*, 2023,49(15):25964-25979.
- [48] MICALLEF C, ZHUK Y, ARIA A I. Recent Progress in Precision Machining and Surface Finishing of Tungsten Carbide Hard Composite Coatings[J]. *Coatings*, 2020,10(8):731.
- [49] ZHAO Z, HUI P, LIU F, et al. Fabrication of niobium carbide coating on niobium by interstitial carburization[J]. *International Journal of Refractory Metals and Hard Materials*, 2020(88):105187.
- [50] KHAN M, AHMAD S, ZAIDI S, et al. Titanium carbide coating on graphene nanoplatelets[J]. *Journal of Materials Research and Technology*, 2020,9(3):3075-3083.
- [51] LIU W, YANG J, QIU Y, et al. Titanium carbide's effects on coatings formed on D16T aluminum alloy by plasma electrolytic oxidation[J]. *Anti-Corrosion Methods and Materials*, 2020,67(1):48-58.
- [52] CHEN Z, LI H, REN L, et al. Effect of Tungsten Carbide Addition on the Wear Resistance of Flame-Sprayed Self-Lubricating Ni-Graphite Coatings[J]. *Journal of Materials Engineering and Performance*, 2020,29(2):1156-1164.
- [53] MEN X, TAO F, GAN L, et al. Erosion behaviour of cobalt-based coatings with different carbide contents under high-speed propellant airflow[J]. *Surface Engineering*, 2020,36(11):1210-1218.
- [54] LI H, YANG X, CHEN Y, et al. Microstructure and properties of Cr-Nb carbide coatings on graphite via powder immersion reaction assisted coating[J]. *Surface and Coatings Technology*, 2023(455):129226.
- [55] PANA I, VLADESCU A, CONSTANTIN L R, et al. In Vitro Corrosion and Tribocorrosion Performance of Biocompatible Carbide Coatings[J]. *Coatings*, 2020,10(7):654.
- [56] GOVANDE A R, RATNA SUNIL B, DUMPALA R. Wear and corrosion behaviour of the cryogenically treated tungsten carbide coatings[J]. *Surface Engineering*, 2023,39(3):326-338.
- [57] KHATER M A, BOUAZIZ S A, GARRIDO M A, et al. Mechanical and tribological behaviour of titanium boride coatings processed by thermochemicals treatments[J]. *Surface Engineering*, 2020,37(1):101-110.
- [58] DIPPO O F, MESGARZADEH N, HARRINGTON T J, et al. Bulk high-entropy nitrides and carbonitrides[J]. *Sci Rep*, 2020,10(1):21288.
- [59] WANG Y, ZHANG B, ZHANG C, et al. Ablation behaviour of (Hf-Ta-Zr-Nb)C high entropy carbide ceramic at temperatures above 2100 °C[J]. *Journal of Materials Science & Technology*, 2022(113):40-47.
- [60] Zhao K, Ye F, Cheng L F, et al. Formation of Ultra-High Temperature Ceramic Hollow Microspheres as Promising Lightweight Thermal Insulation Materials via a Molten Salt-Assisted Template Method[J]. *ACS Applied Material & Interfaces*, 2021,13(32):37388-37397.
- [61] ZHU Y, CHAI J, WANG Z, et al. Microstructural damage evolution of (WTiVNbTa)_{C₅} high-entropy carbide ceramics induced by self-ions irradiation[J]. *Journal of the European Ceramic Society*, 2022,42(6):2567-2576.
- [62] TUNES M A, FRITZE S, OSINGER B, et al. From high-entropy alloys to high-entropy ceramics: The radiation-resistant highly concentrated refractory carbide (CrNbTaTiW)C[J]. *Acta Materialia*, 2023(250):118856.
- [63] HAI Z, ZIHAO W, HAO C, et al. Microstructure, Mechanical and Tribological Properties of High-Entropy Carbide Ceramics (VNbTaMoW)C₅-SiC[J]. *Powder Metallurgy and Metal Ceramics*, 2023,61(7-8):451-458.
- [64] CAI F, NI D, BAO W, et al. Ablation behavior and mechanisms of Cf/(Ti_{0.2}Zr_{0.2}Hf_{0.2}Nb_{0.2}Ta_{0.2})C-SiC high-entropy ceramic matrix composites[J]. *Composites Part B: Engineering*, 2022(243):110177.
- [65] LUO S C, GUO W M, PLUCKNETT K, et al. Low-temperature densification of high-entropy (Ti,Zr,Nb,Ta,Mo)C-Co composites with high hardness and high toughness[J]. *Journal of Advanced Ceramics*, 2022,11(5): 805-813.
- [66] BEILIN YE, TONGQI WEN, MANH CUONG NGUYEN, et al. First-principles study, fabrication and characterization of (Zr_{0.25}Nb_{0.25}Ti_{0.25}V_{0.25})C high-entropy ceramics[J]. *Acta Materialia*, 2019(170):15-23.
- [67] LINDNER T, LÖBEL M, HUNGER R, et al. Boriding of HVOF-sprayed Inconel 625 coatings[J]. *Surface and*

- Coatings Technology, 2020(404):126456.
- [68] MIRHOSSEINI S H, MOSALLAE M, RAZAVI M, et al. Reaction behavior and wear properties of in-situ air plasma-sprayed $\text{Al}_2\text{O}_3\text{-TiB}_2$ composite coatings[J]. Journal of the European Ceramic Society, 2023,43(14):6482-6492.
- [69] ZENG X, LIU Z, TONG X, et al. Preparation and infrared emissivity of metal borides(metal=V,Mo,Fe) and MnO_2 co-doped NiCr_2O_4 coatings[J]. Ceramics International, 2022, 48(4):5581-5589.
- [70] SALYI Z, KAPTAY G, KONCZ-HORVATH D, et al. Boride Coatings on Steel Protecting it Against Corrosion by a Liquid Lead-Free Solder Alloy[J]. Metallurgical and Materials Transactions B, 2022,53(2):730-743.
- [71] ZHANG H, PAN Y, ZHANG Y, et al. Sensitivity Analysis for Process Parameters in Mo_2FeB_2 Ternary Boride Coating by Laser Cladding[J]. Coatings, 2022,12(10):1420.
- [72] BAO J, YU Y, LIU B, et al. In Situ Ternary Boride: Effects on Densification Process and Mechanical Properties of WC-Co Composite Coating[J]. Materials (Basel), 2020,13(8):1995.
- [73] ZHANG H, AKHTAR F. Refractory multicomponent boron-carbide high entropy oxidation-protective coating for carbon-carbon composites[J]. Surface and Coatings Technology, 2021(425):127697.
- [74] KAHL B A, BERNDT C C, ANG A S M. Boride-based ultra-high temperature ceramic coatings deposited via controlled atmosphere plasma spray[J]. Surface and Coatings Technology, 2021(416):127128.
- [75] ÇAKIR M V. A Comparative Study on Tribocorrosion Wear Behavior of Boride and Vanadium Carbide Coatings Produced by TRD on AISI D2 Steel[J]. Protection of Metals and Physical Chemistry of Surfaces, 2022,58(3):562-573.
- [76] LÖBEL M, LINDNER T, HANISCH N, et al. High-temperature wear behaviour of borided Inconel 718 HVOF coatings[J]. IOP Conference Series:Materials Science and Engineering, 2021,1147(1):012032.
- [77] DOÑU RUIZ M A, GARCÍA BUSTOS E D, DE LA MORA RAMIREZ T, et al. Characterization of Boride Coatings on AISI 8620 Steels without and with Hydrogen Permeation[J]. Advances in Materials Science and Engineering, 2022(2022):1-13.
- [78] MAYRHOFER P H, KIRNBAUER A, ERTELHALER P, et al. High-entropy ceramic thin films; A case study on transition metal diborides[J]. Scripta Materialia, 2018(149):93-97.
- [79] ZHANG P, CHENG C, LIU B, et al. Multicomponent $(\text{Hf}_{0.25}\text{Zr}_{0.25}\text{Ti}_{0.25}\text{Cr}_{0.25})\text{B}_2$ ceramic modified SiC-Si composite coatings: In-situ synthesis and high-temperature oxidation behavior[J]. Ceramics International, 2022,48(9):12608-12624.
- [80] GUO L, WANG Y, LIU B, et al. In-situ phase evolution of multi-component boride to high-entropy ceramic upon ultra-high temperature ablation[J]. Journal of the European Ceramic Society, 2023,43(4):1322-1333.

Research and Application of Recycled Concrete Technology in Prefabricated Buildings

Shanshan DENG^{1†}, Gang SHI², Chao SHANG^{3†}, Fuchuan ZHOU^{4*}, Masabo Gasper^{4,5}, Masiko M. Kaziana^{4,5}

1. Chongqing Telecommunication Polytechnic College, Chongqing, 402247, China
2. Chongqing yuxi water conservancy and electric power survey and design institute CO., LTD., Chongqing, 402160, China
3. Chengde Thermal Power Engineering Installation Co., Ltd., Chengde, 067000, China
4. Chongqing Vocational Institute of Engineering, Chongqing, 402260, China
5. Undergraduate Architecture and Civil Engineering, Dar es Salaam Institute of Technology {DIT}, Dar es Salaam, 11103, Tanzania

*Corresponding Author: Fuchuan ZHOU, E-mail: 981480645@qq.com

Abstract

The utilization of waste concrete as a raw material for recycled concrete in the domain of prefabricated components is garnering greater interest. This paper delineates and examines the concept, categorization, methodologies of preparation, applicable sectors, and evaluative metrics of recycled concrete technology, highlighting its prospective benefits. Nonetheless, for the successful integration of recycled concrete technology into prefabricated component applications, it is imperative to systematically enhance its physical, mechanical, and attributes, as well as its environmental efficacy. Moreover, to foster the continued advancement of recycled concrete technology, innovative initiatives, standardization, educational programs, demonstration projects, and collaborative efforts are crucial to promote broader adoption and realize improved outcomes within the realm of prefabricated components. In conclusion, recycled concrete technology is poised to play a pivotal role in prefabricated construction, offering robust support for propelling the construction industry towards a sustainable future.

Keywords: recycled concrete; prefabricated buildings; Environmental performance assessment

1 Introduction

The construction industry's heavy reliance on conventional concrete has amplified resource depletion and environmental consequences. This has paved the way for recycled concrete technology, which recycles and reuses waste concrete to mitigate the need for fresh materials, conserve energy, and substantially reduce the construction sector's environmental footprint^[1-2]. Prefabricated construction has emerged as a cornerstone and direction of modern construction practices, characterized by efficiency, quality control, and sustainability. With the world's urbanization pace accelerating, the construction industry is confronting challenges like resource scarcity, elevated energy use, and increased carbon emissions. In this context, exploring the integration of recycled concrete technology into prefabricated buildings presents a novel avenue for achieving sustainable prefabricated structures.

Prefabricated buildings capitalize on factory-produced, modular components that can be

seamlessly integrated with renewable concrete technology. The controlled factory setting allows for the preparation of recycled concrete, followed by the prefabrication of components, which enhances construction quality and efficiency. The incorporation of recycled concrete into prefabricated facades, floors, and structural systems can bolster building performance and sustainability, while also offering cost savings^[3]. Consequently, there is an immediate necessity for comprehensive performance evaluation, optimization strategies, and environmental impact assessments of recycled concrete technology within prefabricated buildings.

2 Overview of Recycled Concrete Technology

Recycled concrete represents a sustainable alternative in the building industry, derived from waste concrete and construction debris. Processed through crushing, cleaning, and sorting, it serves to mitigate resource waste, lessen environmental impact, and advance sustainable construction practices, positioning it as a material with substantial promise^[4].

Definition and Classification of Recycled Concrete: Recycled concrete is produced by processing waste concrete from structures or construction debris. It can be categorized into three types based on the source and use of the recycled aggregates: recycled coarse aggregate concrete, recycled fine aggregate concrete, and full recycled concrete. Recycled coarse aggregate concrete is primarily composed of recyclable coarse aggregates, while recycled fine aggregate concrete uses recyclable fine aggregates. Full recycled concrete is made from entirely recyclable aggregates recovered from waste concrete structures or construction waste. This material has gained widespread adoption within the construction industry.

The preparation of recycled concrete involves two main steps: collecting and treating waste concrete to produce recycled aggregate, and mixing concrete and performing quality control adjustments to ensure that its quality and performance meet the requirements.

Performance and Characteristics of Recycled Concrete: In the context of prefabricated buildings, the use of recycled concrete is not only about conserving resources and reducing the carbon footprint but also about enhancing building quality and sustainability while potentially lowering construction costs. Through ongoing optimization of its physical, mechanical, durability, and environmental properties, recycled concrete can rival traditional building materials and even offer superior sustainability attributes.

3 Application of Recycled Concrete in Prefabricated Buildings

The integration of recycled concrete technology into prefabricated buildings offers a versatile solution across various components, including exterior wall systems, floor systems, and structural systems. This technology extends beyond traditional applications, providing a array of benefits for construction projects and considerable potential for growth.

3.1 Application of recycled concrete in prefabricated exterior wall systems

The aesthetic appeal, thermal insulation, and overall energy efficiency of a building are crucial to its performance. Recycled concrete technology can be effectively applied to prefabricated exterior wall systems, offering both practical and aesthetic advantages.

Wall Tiles: Recycled concrete wall tiles not only provide excellent thermal insulation but also meet decorative standards, contributing to energy savings.

External Wall Insulation Boards: These boards, made from recycled concrete, enhance thermal insulation properties, reducing building energy consumption and the burden on HVAC systems.

3.2 Application of recycled concrete in prefabricated floor systems

The floor system is a pivotal component of prefabricated buildings, serving both load-bearing and acoustic insulation functions. The adoption of recycled concrete technology in floor systems can enhance their performance, including noise reduction capabilities.

Prefabricated Flooring: Compact and durable recycled concrete floor panels are utilized to bear floor loads, satisfying the mechanical properties and durability requirements of flooring.

Soundproofing Materials: Recycled concrete can be utilized to create soundproofing materials that minimize sound transmission between floors, offering a material-efficient solution that improves the acoustic comfort of residential and commercial buildings.

3.3 Application of recycled concrete in prefabricated components

Prefabricated components are typically produced in a factory setting and then transported to the construction site for assembly into the building's various components. The use of recycled concrete in prefabricated buildings is gaining traction, offering several advantages.

Recycled Concrete Wall Panels: Wall panels made from recycled concrete can reduce the consumption of raw materials while providing comparable strength and stability to traditional concrete panels.

Recycled Concrete Columns and Beams: Recycled concrete is also suitable for manufacturing columns and beams for prefabricated buildings, supporting structural loads and offering cost savings through the use of recycled materials.

Energy-Efficient Wall Systems: Walls constructed with recycled concrete can incorporate heat and sound insulation, contributing to the overall energy efficiency of the building.

The integration of recycled concrete technology into prefabricated buildings represents a promising new direction for the construction industry. It aligns with goals of resource conservation and carbon reduction while enhancing the competitiveness and sustainability of construction projects. However, despite advancements in the mechanical properties, durability, and environmental performance of recycled concrete, further research and practical application are necessary to encourage broader use in prefabricated buildings.

For cast-in-place multi-storey and high-rise recycled concrete houses that use only Class I recycled coarse aggregate, the structural types and maximum heights should adhere to the same standards as those for cast-in-place multi-storey and high-rise ordinary concrete houses^[5]. For buildings using Class II and Class III recycled coarse aggregate, compliance with the structural types and maximum heights specified in Table 1^[6] is required. When the substitution rate of recycled coarse aggregate falls between 30% and 50%, the maximum height applicable can be determined through linear interpolation.

Table 1 Structural types and maximum heights for cast-in-place multi-storey and high-rise recycled concrete houses (m)

| Structure type | Regenerated coarse aggregate substitution rate | Intensity of fortification | | | | |
|---------------------------|--|----------------------------|----|---------|---------|----|
| | | 6 | 7 | 8(0.2g) | 8(0.3g) | 9 |
| Frame structure | 30% | 45 | 40 | 35 | 30 | 21 |
| | 50% | 40 | 35 | 30 | 25 | 15 |
| Frame-shear structure | 30% | 90 | 85 | 70 | 60 | 35 |
| | 50% | 70 | 65 | 55 | 45 | 25 |
| Shear wall structure | 30% | 100 | 85 | 70 | 60 | 45 |
| | 50% | 80 | 70 | 60 | 50 | 35 |
| Frame-core tube structure | 30% | 110 | 90 | 75 | 65 | 50 |
| | 50% | 90 | 75 | 65 | 55 | 40 |

Note: (1) House height refers to the height of the outdoor ground floor to the top of the main roof slab, excluding the local protruding roof Part; (2) The frame in the table includes the special-shaped column frame with no more than six layers and no more than 18m height, excluding other special-shaped column frames; (3) For buildings exceeding the height in the table, special research and demonstration should be carried out to take effective strengthening measures.

4 Performance Evaluation and Optimization of Recycled Concrete Technology

The performance evaluation and optimization of recycled concrete technology are essential to ensure its successful application in prefabricated buildings. This process involves a comprehensive assessment of the physical, mechanical, durability, and environmental properties of the fabricated components it produces.

4.1 Evaluation of physical properties of recycled concrete prefabricated components

The physical properties of recycled concrete, such as density, porosity, and water absorption, are crucial indicators that directly impact its engineering application and performance. Density and Porosity: The density and porosity of recycled concrete are indicative of its quality and compactness. To optimize these characteristics, it is essential to control the concrete preparation process, ensuring thorough vibration and complete filling.

Water Absorption: Water absorption is a critical factor affecting the durability of recycled concrete. The use of appropriate impermeable agents and sealing materials can minimize pores and microcracks, consequently reducing water absorption.

4.2 Evaluation of mechanical properties of recycled concrete

To assess the mechanical properties of recycled concrete, it is essential to determine its compressive strength, tensile strength, and flexural strength, as these indicators are

crucial for ensuring the safety and reliability of the structure. The standard deviation of strength must adhere to the specifications outlined in Table 2^[7].

Compressive strength: The compressive strength of recycled concrete can be effectively enhanced through stringent control measures. Additionally, the utilization of high-performance gel materials can further bolster compressive strength.

Tensile strength: While the tensile strength of typical recycled concrete tends to be lower, it can be enhanced by incorporating fiber materials or employing specialized strengthening techniques.

Flexural strength: Flexural strength, an important parameter for evaluating concrete performance under bending loads, plays a significant role in structural integrity. Achieving favorable flexural resistance necessitates the selection of appropriate concrete mix proportions and strengthening strategies. The onset of quality issues like cracks can substantially compromise the concrete's bending strength.

Table 2 Standard deviation of recycled concrete strength σ (Mpa)

| Strength class | $\leq C20$ | C25~C45 | C50~C55 |
|----------------|------------|---------|---------|
| σ | 4.0 | 5.0 | 6.0 |

4.3 Durability evaluation of recycled concrete

The assessment of the durability of recycled concrete includes evaluating freeze-thaw resistance, sulfate resistance, and chloride ion permeability through testing. These performance indicators are directly linked to the service life and maintenance expenses of concrete structures. It is recommended to incorporate an air-entraining agent in freeze-resistant recycled concrete of grade F100. Additionally, antifreeze solutions containing chlorine salts should not be utilized in reinforced recycled concrete. Table 3^[7] details the specifications for water-to-binder ratio and minimum cementitious material dosage for recycled concrete with varying frost resistance grades.

Table 3 Maximum water-binder ratio and minimum amount of cementing material

| Design frost resistance grade | Maximum water-binder ratio | | Minimum amount of cementing material (kg/m ³) |
|-------------------------------|----------------------------|-----------------------|---|
| | No entrainment agent | Air entrainment agent | |
| F50 | 0.5 | 0.55 | 300 |
| F100 | 0.45 | 0.50 | 320 |

Freeze-thaw Resistance: The freeze-thaw durability of recycled concrete can be enhanced by incorporating antifreeze agents and optimizing the particle size distribution.

Sulphate Resistance: For concrete subjected to sulphate attack, it is crucial to employ a well-designed recycled concrete mix, particularly by utilizing cementing materials that exhibit high sulphate resistance.

Chloride Ion Permeability Resistance: To improve the resistance of recycled concrete against chloride ion penetration, the use of chloride ion inhibitors and appropriate sealing treatments can be beneficial. The fundamental durability requirements for recycled concrete intended for structural applications are outlined in Tables 4 and 5^[7].

Table 4 Basic requirements for durability of recycled concrete used in structures

| Environmental grade | Maximum water-binder ratio | Minimum strength class | Maximum chloride content (%) | Maximum alkali content (kg/m ³) |
|---------------------|----------------------------|------------------------|------------------------------|---|
| 1 | 0.6 | C25 | 0.3 | No limit |
| 2 | a | C30 | 0.2 | 3.0 |
| | b | C35(C30) | 0.15 | |
| 3 | a | C40(C35) | 0.15 | 3.0 |
| | b | C45 | 0.10 | |

Table 5 Maximum water-binder ratio of impermeable recycled concrete

| Design impermeability grade | Strength grade of concrete | |
|-----------------------------|----------------------------|---------|
| | C20~C30 | C35、C40 |
| P6 | 0.55 | 0.50 |
| P8~P12 | 0.50 | 0.45 |
| >P12 | 0.45 | 0.40 |

4.4 Environmental performance assessment of recycled concrete

The environmental assessment of recycled concrete technology encompasses evaluations of carbon footprint, energy efficiency, and life cycle analysis. These assessments are critical in determining the environmental impact of recycled concrete and in providing data that supports sustainable construction practices.

Carbon Footprint: Assessing the carbon emissions of recycled concrete relative to conventional concrete allows for conclusions regarding its environmental impact. The goal is to reduce carbon emissions by incorporating energy-efficient technologies into the production process and by utilizing low-carbon concrete formulations.

Energy Efficiency: Energy efficiency is a key component of sustainable development, affecting both the preparation of concrete and the construction process. The use of energy-saving technologies, such as those that harness renewable energy, can enhance overall energy efficiency.

Life Cycle Analysis: Life cycle analysis considers the environmental impact of concrete across all stages, including production, preparation, transportation, construction, and maintenance. By optimizing these stages, it is possible to improve the overall

environmental performance of concrete.

5 Conclusion

Recycled concrete is a kind of sustainable building material that has attracted widespread interest in the field of prefabricated construction and has been applied to some extent. Recycled concrete technology offers a potential solution for sustainable construction by recycling and reusing discarded concrete. This paper deeply studies and discusses the definition, classification, preparation method, performance evaluation, application and optimization strategy of recycled concrete technology.

Although there is great potential for recycled concrete technology in prefabricated buildings, there are still challenges to be overcome in terms of standardization, innovation, education and training, demonstration projects and cooperation. In the future, we believe that recycled concrete technology will continue to play an even greater role in prefabricated construction, leading the construction industry towards a more sustainable future while contributing to environmental protection and resource conservation.

Acknowledgements: Supported by the Science and Technology Research Program of Chongqing Municipal Education Commission (Grant No.KJQN202204305, and No.KJQN202305501).

References

- [1] Wu Lina. Research on carbon emission reduction path of low-carbon building construction and construction under dual-carbon background [J]. Heilongjiang Environmental Bulletin, 2019,36(5):33-35.
- [2] Li Shifu, Cui Yongjuan, Guo Li. Case study of prefabricated building structure design [J]. Jushe, 2024(11):136-139.
- [3] Guo Kunpeng, Li Qun, Liu Jianfeng. Research and application of recycled concrete technology in prefabricated buildings[J]. Engineering and Construction, 2019,34(4):710-711,717.
- [4] Liu Han. The prospect and application of green concrete analysis [J]. Journal of anhui construction, 2019,26 (4): 194-195.
- [5] Chen Lingling, Cao Xingyu, Wang Zhiyuan, et al. Construction preparation of solid waste recycled concrete technology application research review[J]. Journal of shanxi building, 2023,49(8):29-32.
- [6] Ministry of Housing and Urban Rural Development of the People's Republic of China. Technical standard for recycled concrete structures: JGJT 443-2018[S]. Beijing. China Construction Industry Press, 2018:15.
- [7] Shandong Provincial Department of Housing and Urban Rural Development. Specification for mix proportion design of recycled concrete: DB37/T 5176—2021[S]. Beijing. China Construction Industry Press, 2021:13,32-35.

Publisher: Viser Technology Pte. Ltd.

URL: www.viserdata.com

Add.:21 Woodlands Close, #08-18,

Primz Bizhub SINGAPORE (737854)

